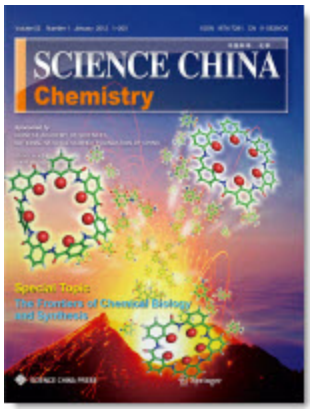

Ultrastrong room-temperature phosphorescence in cucurbit[8]uril-mediated crystalline supramolecules for ratiometric detection of phenethylamine

Journal:	*SCIENCE CHINA Chemistry*
Manuscript ID	SCC-2024-1115.R2
Manuscript Type:	Article
Date Submitted by the Author:	06-Nov-2024
Complete List of Authors:	Niu, Qingyu; Hebei University of Technology, School of Chemical Engineering and Technology Ye, Yingxiang; Fujian Normal University, College of Chemistry and Materials Science Su, Lingna; Hebei University of Technology, School of Chemical Engineering and Technology He, Xu; Hebei University of Technology, School of Chemical Engineering and Technology Li, Zhiqiang; Hebei University of Technology, School of Chemical Engineering and Technology Liu, Yu
Keywords:	room-temperature phosphorescence, cucurbituril, host-guest complex, crystalline, ratiometric detection
Speciality:	Analytical Chemistry
Note: The following files were submitted by the author for peer review, but cannot be converted to PDF. You must view these files (e.g. movies) online.	
BPBA-CB8.cif Scheme Figures and TOC.rar	

https://www.sciengine.com/doi/10.1007/s11426-024-2410-x

SCIENCE CHINA
Chemistry

• ARTICLES •

Ultrastrong room-temperature phosphorescence in cucurbit[8]uril-mediated crystalline supramolecules for ratiometric detection of phenethylamine

Qingyu Niu,[1+] Yingxiang Ye,[2+] Lingna Su,[1] Xu He,[1] Zhiqiang Li[1,3]* & Yu Liu[4]*

[1]*School of Chemical Engineering and Technology, Hebei University of Technology, GuangRong Dao 8, Hongqiao District, Tianjin 300130, P. R. China*

[2]*Fujian Provincial Key Laboratory of Polymer Materials, College of Chemistry and Materials Science, Fujian Normal University, Shangsan Road 8, Cangshan District, Fuzhou, Fujian 350007, China*

[3]*Key Laboratory of Advanced Energy Materials Chemistry (Ministry of Education), Nankai University, Tianjin 300071, China*

[4]*College of Chemistry, State Key Laboratory of Elemento-Organic Chemistry, Nankai University, Weijin Road 94, Nankai District, Tianjin 300071, P. R. China*

Received ***; accepted ***; published online ***

It is a great challenge to modulate purely organic fluorescence-phosphorescence dual emission in aqueous solution because the excited singlet and triplet states are in competition with each other. Herein, we report a crystalline 1:2 host-guest formed by self-assembly of 4-(4-bromophenyl)-pyridinium derivatives and cucurbit[8]uril, in which a rigid environment rich in weak interactions is directly demonstrated. Due to the inhibition of non-radiative transition and stabilization of triplet exciton in the crystalline environment, the crystalline inclusion complex exhibits ultralong room-temperature phosphorescence lifetime of 3.21 ms with an RTP quantum yield up to 16.29%. Interestingly, the crystalline 1:2 host-guest complex demonstrates the ability of rapid identification and sensitive fluorescence-phosphorescence ratiometric detection behavior toward phenethylamine, a drug analogue, with a limit of detection as low as 27.5 nM. We believe that this study will undoubtedly broaden the utilizing scopes of RTP and offers a novel avenue for psychoactive substances monitoring.

room-temperature phosphorescence, cucurbituril, host-guest complex, crystalline, ratiometric detection

Citation: Niu QY, Ye YX, Su LN, He H, Li ZQ, Liu Y. Title: Ultrastrong room-temperature phosphorescence in cucur-bit[8]uril-mediated crystalline supramolecules for ratiometric de-tection of phenethylamine. *Sci China Chem*, ***, doi: ***

1 Introduction

Taking drugs can provide individuals with a temporary euphoria, but it can also cause serious and irreversible harm to the body's physiology.[1] Synthetic drugs, including methamphetamine (crystal meth) or MDMA (ecstasy), have led to a variety of criminal activities that are a global social issue due to their addictive properties.[2] The detection of drugs and their analogues has garnered significant attention. Phenylethylamine (PEA) is an appropriate model compound, given that its derivatives encompass substances with these potential for abuse, such as methamphetamine and MDMA.[3] The methods used to detect PEA-type drugs or their analogues primarily include high-performance liquid

*Corresponding authors (email: zhiqiangli@hebut.edu.cn; yuliu@nankai.edu.cn)

Niu QY and Ye YX contributed equally to this work.

chromatography and electrochemical detection, which are rely on the expensive equipment or specialized operators.[4-6] Luminescent detection, particularly ratiometric luminescent detection, enables straightforward and rapid on-site monitoring of analytes with self-calibration and high accuracy.[7-10] Compared with monotonic fluorescence signal channel, the fluorescence-phosphorescence dual-signal output ratiometric probe demonstrates ultra-high sensitivity due to the sensitive triplet exciton.[11] Meanwhile, the long-lifetime phosphorescence results in high signal-to-noise ratio, which reduces the influence of background fluorescence signal and environmental conditions.[12-14] Therefore, fluorescence-phosphorescence dual-signal output is an ideal candidate for the construction of ratiometric probes.

Traditional dual-emission materials that exhibit both fluorescent and phosphorescent properties are typically composed of precious metal complexes, which are expensive and potentially toxic.[15,16] In contrast, purely organic room-temperature phosphorescence (RTP) materials with dual-emission properties are relatively rare,[17,18] since the weak spin-orbit coupling of organic molecules leads to a weak intersystem crossing (ISC) process.[19-21] Especially in aqueous condition, most organic RTP are quenched by water molecules and other quenchers, limiting their application in luminescent detection.[22] Notably, in purely organic molecules, the excited singlet and triplet states compete with each other.[23] Therefore, regulating dual-emission of fluorescence and phosphorescence in aqueous solution presents a daunting challenge.

Promoting ISC process and limiting non-radiative transition are two general methods for achieving efficient long lifetime organic RTP emission.[24,25] Solid organic RTP materials have been produced through various methods, including polymer confinement,[26-28] halogen bonding,[29,30] host-guest self-assembly,[31,32] etc. Among them, the host-guest inclusion complex between cucurbit[8]uril (CB[8]) and 4-(4-bromophenyl)-pyridinium derivatives is a classic example of aqueous RTP material, where the encapsulation of CB[8] promotes dimeric assembly of 4-(4-bromophenyl)-pyridinium moiety, effectively inhibiting molecular motion of the guest and preventing quenching effect from water.[33-35] Furthermore, the crystallization-induced phosphorescence exhibited qualitative improvements in comparison to the self-assembly in solution process, attributed to the rigid crystalline environment that the guest is subjected to.[36] Meanwhile, unambiguous crystalline structures provide an opportunity to explore the mechanism of RTP emission in-depth, and allow a better understanding of the structural-functional relationships and promote further development in this field. However, crystalline RTP materials based on host-guest self-assembly remain very limited.[36,37]

Herein, we report an RTP enhancement in a crystal of 4-(4-bromophenyl)-pyridinium carboxylic acid (BPBA) and CB[8] inclusion complex. This host-guest complex enables sensitive ratiometric detection of phenylethylamine in water by dual-signal output of fluorescence and phosphorescence (Scheme 1). A 1:2 host-guest complex is formed by self-assembly of BPBA and CB[8] in water. The tight stacking of the guest and the confinement of the hydrophobic CB[8] cavity synergistically inhibit the molecular motion of the guest and prevent triplet exciton from quenchers in water, thereby inducing RTP emission in aqueous phase. While the host-guest crystals provide a more rigid microenvironment rich in weak interactions, including hydrogen bonding, halogen bonding, and strong ion-dipole interactions, which efficiently promote the ISC process and suppress the non-radiative transitions of the guest molecules, resulting in a significant enhancement in RTP efficiency. As a result, compared with the soluble BPBA□CB[8] inclusion complex, the RTP lifetime of the $(BPBA)_2$·CB[8] crystal is extended from 0.342 to 3.21 ms with the RTP quantum yield increasing from 1.60% to 16.29%, setting up a new benchmark for macrocyclic confined RTP materials. In particular, the obtained crystalline host-guest complex exhibits fluorescence-phosphorescence ratiometric detection behavior toward PEA with high sensitivity and excellent selectivity. Finally, this fluorescence-phosphorescence ratiometric sensor is equipped to lateral flow immunoassay (LFIA) strip for on-site visual detection of phenethylamine. The results presented here demonstrate the great potential of macrocyclic confined RTP materials as sensors for psychoactive substances, which will undoubtedly broaden the application scope of RTP.

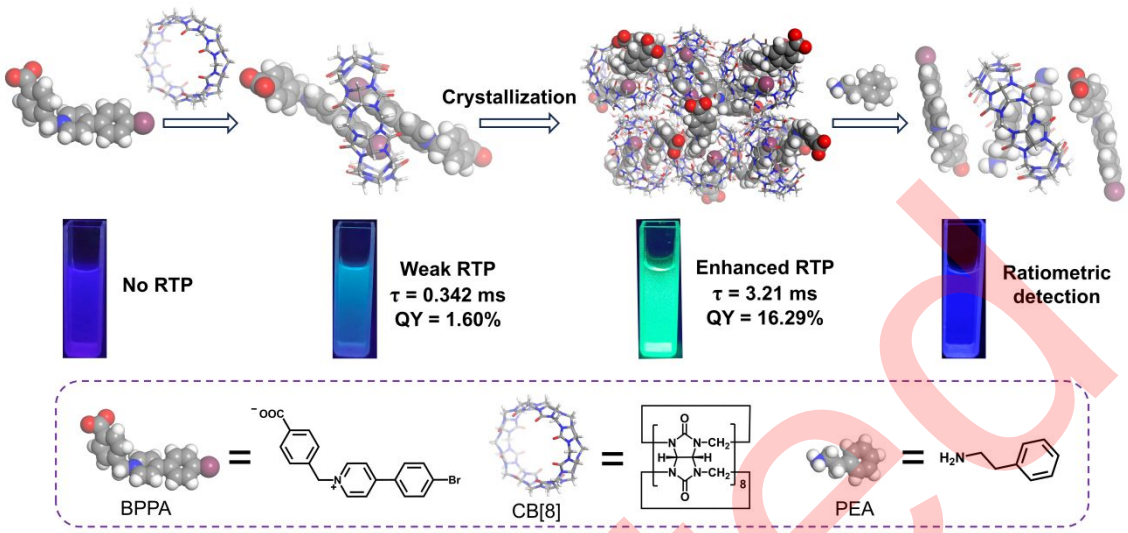

Scheme 1 Schematic illustration of the construction of crystalline host-guest RTP material and its ratiometric detection of phenethylamine.

2 Experimental

2.1 Materials

All chemical reagents were purchased commercially and used directly without further purification. 4-(4-Bromophenyl)pyridine and 4-(Chloromethyl)benzoic acid were purchased from Shanghai Bide Pharmaceutical Technology Co., Ltd. CB[8] and CB[7] were purchased from Beijing HWRK Chem Co., Ltd.

2.2 Synthesis of compound BPBA

4-(4-Bromophenyl)pyridine (200 mg, 0.85 mmol) and 4-(Chloromethyl)benzoic acid (170.6 mg, 1 mmol) was dissolved in CH_3CN (15 mL). The mixture was heated at 80 °C for 24 h. After cooled to room temperature, the precipitate was filtrated and washed with diethyl ether to afford a white solid (237 mg, 0.59 mmol, 70%). ^{1}H NMR (400 MHz, DMSO-d_6) δ 13.12 (s, 1H), 9.26 (d, J = 6.4 Hz, 2H), 8.57 (d, J = 6.4 Hz, 2H), 8.02 (dd, J = 13.3, 8.2 Hz, 4H), 7.87 (d, J = 8.4 Hz, 2H), 7.65 (d, J = 8.0 Hz, 2H), 5.94 (s, 2H). ^{13}C NMR (100 MHz, DMSO-d_6) δ 167.23, 154.64, 145.64, 139.42, 133.16, 132.02, 130.76, 130.52, 129.26, 126.91, 125.52, 62.48. LC-MS m/z for $C_{19}H_{15}BrClNO_2^+$ calcd. $[M - Cl]^+$: 368.0281; found: 368.0281. FTIR (inter alia): 3421, 1686 cm^{-1} (O-H, C=O stretches).

3 Results and discussion

3.1 Host-guest self-assembly behavior

BPBA was readily synthesized by reacting 4-(4-bromophenyl)pyridine with 4-(chloromethyl)benzoic acid (Scheme S1, Figures S1-S4, Supporting Information). Then, the assembly behavior of CB[8] and BPBA in water was comprehensively investigated. ^{1}H NMR titration experiments showed that the protons of bromophenyl unit (H_1 and H_2) exhibited significant upfield shifts (Δδ = 1.22 ppm and 1.13 ppm, respectively) upon the addition of CB[8] (Figure 1a), revealing that the bromophenyl unit was deeply included in the cavity of CB[8].[36] In addition, the protons of pyridinium unit (H_3 and H_4) shifted to upfield slightly (Δδ = 0.52 ppm and 0.04 ppm, respectively), suggesting that it was located near the portal inside the CB[8] cavity.[38] In contrast, the protons of benzoate moiety (H_6 and H_7) shifted to downfield (Δδ = 0.18 ppm and 0.04 ppm, respectively), indicating that the benzoate moiety was located outside the CB[8] cavity.[39] Meanwhile, both free and bound BPBA protons appeared after the addition of 0.25 eq. CB[8], indicating the slow exchange kinetics of this recognition process. As shown in Figure 1c, with the addition of CB[8], the absorption peak of BPBA shifted from 308 to 313 nm, and its absorbance intensity decreased with isosbestic points appeared at 234, 252 and 327 nm. Because a possible reason may be that BPBA forms host-guest complex with CB[8] in water with a new host-stabilized charge-transfer state.[36] Job's plot

determined by UV absorption spectra showed a maximum value at X_{BPBA} ([BPBA]/([BPBA] + [CB[8]])) = 0.67, preliminarily indicating that two BPBA molecules were encapsulated by one CB[8] to form a 1:2 complex (Figure S5). Meanwhile, electrospray ionization mass spectrometry (ESI-MS) spectrum showed the ion peak at 1033.5707 corresponded to $[2BPBA + CB[8] - 2Cl]^{2+}$ (1033.2234), further confirming the formation of a stable 1:2 complex (Figure S6). In addition, two-dimensional rotating frame Overhauser effect spectroscopy (2D ROESY) demonstrated the presence of strong correlation signals between H_1-H_2, which suggests that the bromophenyl unit in the CB[8] cavity adopts a head-to-tail stacking mode (Figure 1b). The corresponding two step binding constants were calculated as $K_1 = 2.03 \times 10^5$ M^{-1} and $K_2 = 3.23 \times 10^4$ M^{-1} according to the UV-vis absorption titration (Figure 1d).

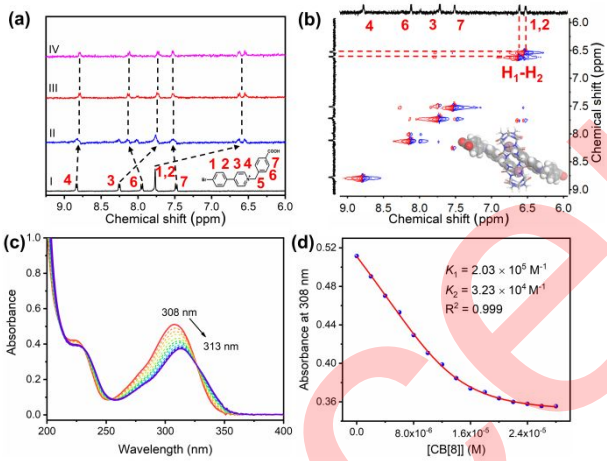

Figure 1 The host-guest binding behavior. (a) ^{1}H NMR titration spectra (400 MHz, D_2O, 298 K) of BPBA (1.2 mM) upon addition of (I) 0, (II) 0.25, (III) 0.50 and (IV) 1.0 eq. of CB[8]. (b) 2D ROESY spectrum of BPBA□CB[8] ([BPBA] = 2[CB[8]] = 1.2 mM). (c) The UV-vis absorption spectra of BPBA (20 μM) upon the addition of CB[8] (0-1.4 eq.) and (d) the corresponding binding constants.

3.2 Photoluminescence behavior of BPBA□CB[8]

We further studied the photoluminescence behavior of the BPBA□CB[8] complex in aqueous solution. As shown in Figure 2a, free BPBA showed a blue emission centered at around 387 nm. With the stepwise addition of CB[8] (0-1.0 eq.), a new emission peak appeared at 500 nm, accompanied by a decrease in emission at 387 nm. Meanwhile, a change in luminescence emission color from blue to green could be observed with the naked eye. The corresponding Commission International del'Eclairage (CIE) coordinates are displayed in Figure 2b. It is worth noting that a significant enhancement was observed specifically in the green emission under N_2 atmosphere, while no change was observed in the emission at 387 nm (Figure S7a). Subsequently, transient spectra were performed with a delay of 0.5 ms to demonstrate the property of the green emission band. Green emission at 500 nm was only observed in the BPBA□CB[8] complex, rather than in free BPBA (Figure 2c). The lifetime measured at 387 nm was on a nanosecond scale, with lifetimes of 0.40 and 0.42 ns assigned to free BPBA and the BPBA□CB[8] complex, respectively (Figure S7b, c). In contrast, the BPBA□CB[8] complex exhibited a long lifetime of 0.342 ms when monitored at 500 nm (Figure 2d). Moreover, under N_2 atmosphere, BPBA□CB[8] exhibited a significant increase in emission intensity at 500 nm and longer lifetime of 1.20 ms in water (Figure 2c, d). Meanwhile, the delayed emission at 500 nm exhibited a thermally quenched property (Figure S8), thus, the green emission at 500 nm can be attributed to RTP. To examine the correlation between assembly mode and luminescence properties, we conducted a control experiment using CB[7] that mainly forms 1:1 inclusion complex with guest molecule. As expected, Job's plot showed a maximum value at X_{BPBA} ([BPBA]/([BPBA] + [CB[7]])) = 0.5, revealing that BPBA was encapsulated in the smaller cavity of CB[7] to form a 1:1 host-guest complex (Figure S9a, b). UV-vis spectroscopic titration also showed a red shift from 308 to 313 nm with a decrease in intensity (Figure S9c). In addition, as shown in Figure S9d, the fluorescence emission at 387 nm increased with the addition of CB[7], meanwhile, no phosphorescence emission was observed under environmental conditions. These results indicate that the macrocyclic encapsulation of CB[8] and the dimeric assembly of BPBA restrict the molecular motion of the guest and prevent the quenching effect of oxygen and water, thereby inducing RTP emission in aqueous solution.[40] In a control test, the photoluminescence spectra of BPBA powder showed a blue emission at 464 nm (Figure S10a). As illustrated in Figure S10b, a weak RTP emission at 562 nm with a lifetime of 0.709 ms was observed in the delayed spectrum of solid-state BPBA powder, indicating the RTP enhancement at confined solid-state.

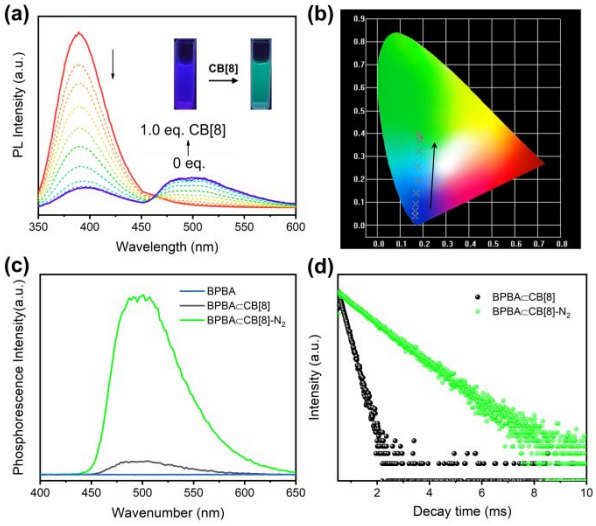

Figure 2 The photoluminescence behavior of the BPBA□CB[8] complex in water. (a) The photoluminescence spectra (λ_{ex}= 330 nm) of BPBA (20 μM) upon the addition of CB[8] (0-1.0 eq.) and (b) the corresponding CIE chromaticity diagram (λ_{ex}= 330 nm, [BPBA] = 20 μM). Inset: The photos of BPBA before and after the addition of 1.0 eq. CB[8]. (c) The RTP emission of free BPBA, BPBA□CB[8] under air condition and N_2 atmosphere and (d) the corresponding RTP decay curves (λ_{ex}= 330 nm, [BPBA] = 2[CB[8]] = 20 μM). The y-axis of Figure 2d is presented in a logarithmic scale.

3.3 Single crystal structure analysis

Colorless rod-like single crystal of $(BPBA)_2$·CB[8] suitable for X-ray diffraction analysis was obtained by mixing BPBA and CB[8] in aqueous solution at room temperature (Supporting Information, Figure S11). Host-guest complex $(BPBA)_2$·CB[8] crystallized in the triclinic space group *P*-1 (Table S1), with four distinct CB[8] fragments and four different BPBA molecules in the asymmetric unit. There are four different conformations of BPBA (named BPBA-a, -b, -c, -d, respectively, Figure 3b) in the $(BPBA)_2$·CB[8] crystal, and two conformation identical BPBA are paired with CB[8] to form four types of homologous ternary host-guest complexes. As illustrated in Figure 3a, the 4-bromophenyl units of a pair of BPBA are located within the cavity of CB[8] through a head-to-tail stacking mode, while the benzoate units are exposed, which is well consistent with the analysis of the ^{1}H NMR titration. Importantly, since two 4-bromophenyl groups of the two BPBA molecules are confined inside the CB[8] cavity, the π-π interactions are observed in the $(BPBA)_2$·CB[8] crystal. The centroid-centroid distances between the parallel benzene rings of BPBA ranges from 3.755 Å to 4.200 Å in these homologous complexes (Figure 3c). In addition, multiple C-H···O/N interactions (2.357 to 3.601 Å), -Br···N- halogen bonds (3.351 to 3.439 Å), and strong ion-dipole interactions (3.009 to 4.078 Å) are synergistically to stabilize the ternary host-guest complex (Figure S12). Each $(BPBA)_2$·CB[8] unit can connect adjacent CB[8] units through multiple hydrogen bonds and van der Waals interactions to form a two-dimensional layer structure parallel to the *bc* plane. Finally, large number of free water molecules interact with carboxylate and CB[8] through multiple hydrogen bonds interactions to connect the adjacent two-dimensional layers into a three-dimensional packing structure (Figure S13).

The powder X-ray diffraction (PXRD) pattern of the as-synthesized $(BPBA)_2$·CB[8] matches well with the simulated results from single crystal X-ray diffraction (Figure S14), indicating its high purity. Energy dispersive X-ray spectroscopy (EDS) mapping revealed the absence of Cl^- in the $(BPBA)_2$·CB[8] crystal (Figure S11). This finding is consistent with the previous work, indicating that BPBA is deprotonated in the crystal structure, as observed in the single crystal structure analysis.[37] In addition, thermogravimetric analysis (TGA) of $(BPBA)_2$·CB[8] showed approximate 12.2% weight loss before 150 ℃ (Figure S15), corresponding to the loss of crystalline water molecules (calcd 11.7%). Acid-digested ^{1}H NMR integral further confirmed that the molar ratio of CB[8] and BPBA in $(BPBA)_2$·CB[8] was nearly 1:2 (Figure S16), which is highly consistent with the results of single crystal data.

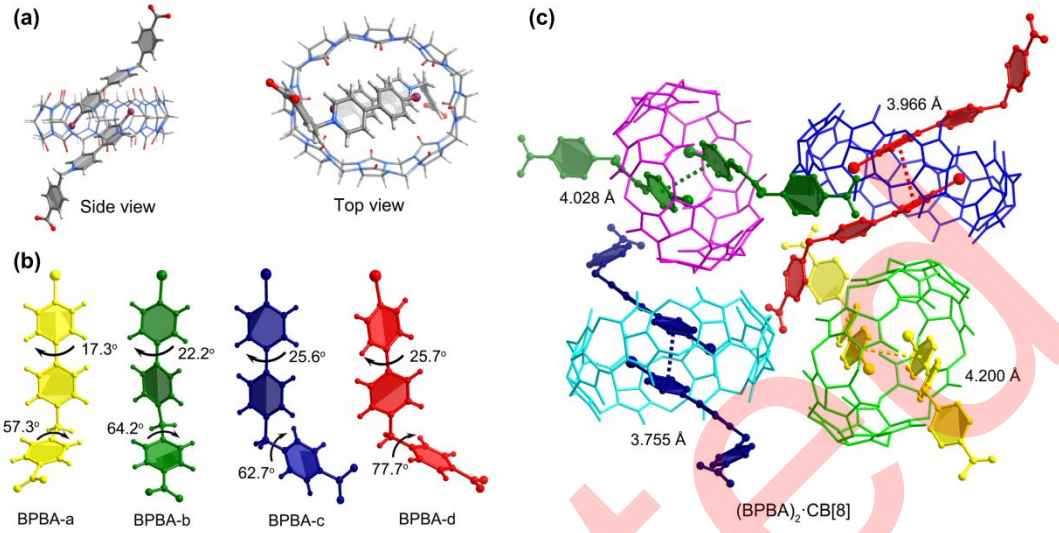

Figure 3 Crystal structure of $(BPBA)_2$·CB[8]. (a) Side view and top view of $(BPBA)_2$·CB[8]. (b) Four different types of conformations of BPBA in the $(BPBA)_2$·CB[8] complex (named BPBA-a, BPBA-b, BPBA-c, and BPBA-d). (c) Partial molecular packing of $(BPBA)_2$·CB[8], and the π-π interactions of a pair of BPBA molecules inside the CB[8] cavity are presented. Hydrogen atoms and free water molecules are omitted for clarity.

3.4 Photoluminescence properties of $(BPBA)_2$·CB[8] crystal

Subsequently, the photoluminescence behaviors of $(BPBA)_2$·CB[8] crystal were also investigated. $(BPBA)_2$·CB[8] crystal was dispersed in water and then ultrasound was employed to produce a water suspension with a concentration of 50.0 μg/mL (Supporting Information). The steady-state photoluminescence spectrum of $(BPBA)_2$·CB[8] water suspension showed double emission peaks at 387 and 500 nm. The emission peak at 500 nm is stronger and corresponds to the bright green emission under a 302 UV lamp (Figure 4a). Meanwhile, the phosphorescence spectrum of $(BPBA)_2$·CB[8] water suspension only displayed the green emission band at around 500 nm, while the blue emission band was absent (Figure 4a-c). This reveals the blue fluorescence and green RTP dual-emission behavior of $(BPBA)_2$·CB[8]. Compared with the excitation peak of free BPBA (λ_{ex}=325 nm), the excitation peaks of BPBA□CB[8] solution and $(BPBA)_2$·CB[8] crystal exhibited a stepwise red shift to 330 and 345 nm, respectively (Figure S17a). After assembled into crystal, the phosphorescence emission intensity showed a significant enhancement with I_{387}/I_{500} decreased from 71.1 to 0.68, the RTP lifetime prolonged from 0.342 to 3.21 ms, and the quantum yield of RTP increased from 1.60 to 16.29% (Figure 4d-f, Figure S17b, c). Even in presence of water, the $(BPBA)_2$·CB[8] suspension exhibited a high RTP quantum yield of 14.72% and lifetime of 2.03 ms. Notably, when considering both lifetime and quantum yield, the RTP performance of this crystalline host-guest complex is superior to all of previously reported CB[8] confined host-guest complexes in aqueous solution (Figure 4g and Table S2), and the RTP lifetime is next only to that of CB[8]/polymer co-confined system, thus setting up a new benchmark in macrocyclic confined RTP materials.[41]

To understand the phosphorescence enhancement mechanism, the intersystem crossing rate (k_{isc}), radiative and nonradiative decay rate constants (k_r^{phos} and k_{nr}^{phos}) were calculated through the obtained quantum yields and lifetime. As expected, $(BPBA)_2$·CB[8] crystal showed a k_{isc} of 3.88 × 10^8 s^{-1}, an order of magnitude higher than that of BPBA□CB[8] aqueous inclusion complex (3.40 × 10^7 s^{-1}) (Figure 4h). Encouragingly, the k_{nr}^{phos} of $(BPBA)_2$·CB[8] (261 s^{-1}) was much lower than that of BPBA□CB[8] (2880 s^{-1}) (Figure S18a). It is widely recognized that high RTP efficiency (k_r^{phos} /(k_r^{phos} + k_{nr}^{phos}) results in a high RTP quantum yield, while a long lifetime is based on a small (k_r^{phos} + k_{nr}^{phos}).[41] Compared with BPBA□CB[8], $(BPBA)_2$·CB[8] exhibited a much larger (k_r^{phos} /(k_r^{phos} + k_{nr}^{phos})) and smaller (k_r^{phos} + k_{nr}^{phos}) (Figure 4i and Figure S18b). This phenomenon demonstrates that crystallization could effectively promote ISC process, increase the

radiative decay channels and inhibit non-radiative transition of BPBA, thus significantly improve the RTP performance in aqueous solution.

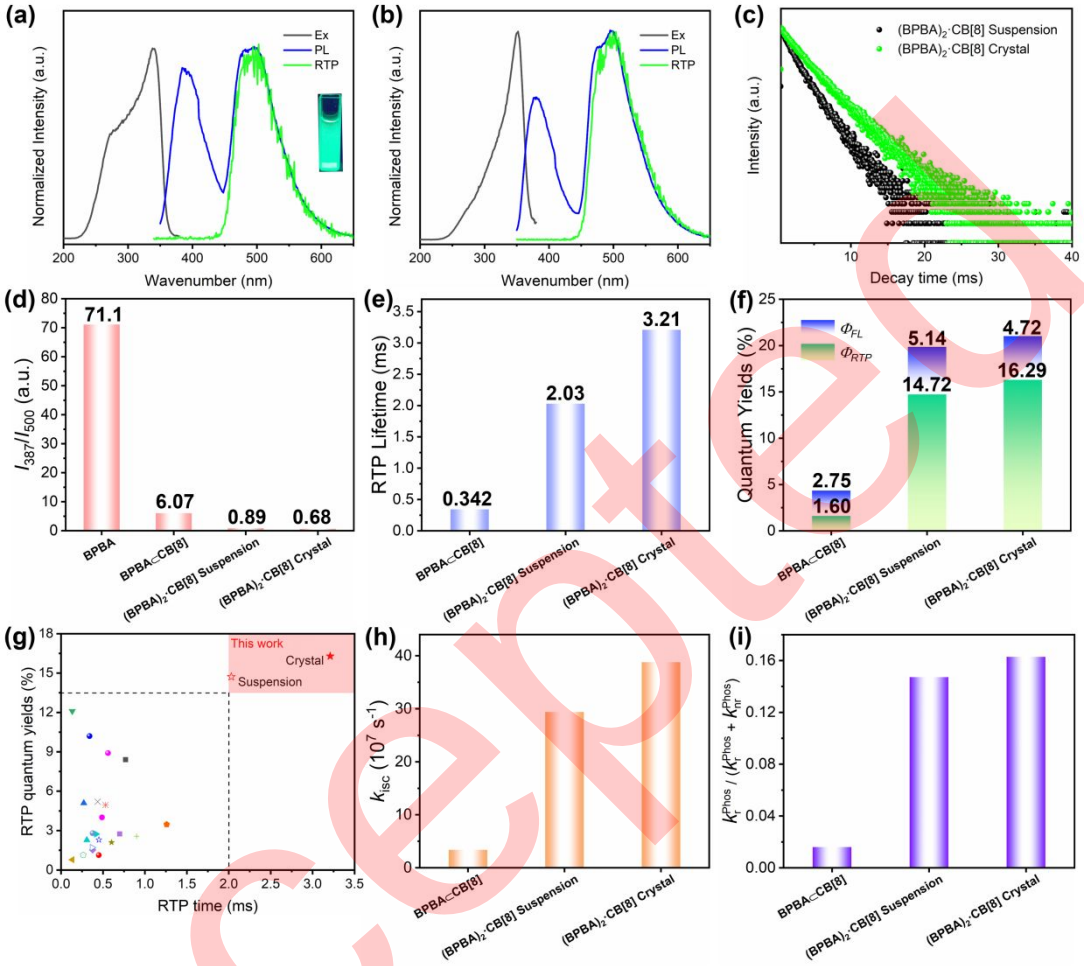

Figure 4 The photoluminescence behavior of $(BPBA)_2$·CB[8] crystal. Normalized excitation, photoluminescence (λ_{ex}= 345 nm) and RTP spectra (delayed by 0.5 ms) of $(BPBA)_2$·CB[8] water suspension (a) and in crystal state (b), and (c) the corresponding RTP decay curves. Inset: The photos of $(BPBA)_2$·CB[8] water suspension. (d-f) The I_{387}/I_{500}, RTP lifetime and quantum yields of different samples. (g) Comprehensive comparison of RTP lifetime and quantum yields in this work and previous reported CB[8] confined host-guest complexes in aqueous solution (for detail in Table S2). The y-axis of Figure 4c is presented in a logarithmic scale. (h, i) The photophysical parameters of different samples.

3.5 Ratiometric photoluminescent detection behavior to PEA

Given CB[8]'s strong bind ability to positively charged substances, we investigated the potential of $(BPBA)_2$·CB[8] in ratiometric photoluminescent detection of PEA in aqueous solution. Firstly, the conditions for the detection of $(BPBA)_2$·CB[8] toward PEA were optimized. For convenience, all the analytical experiments were conducted at room-temperature. The photoluminescent spectra of $(BPBA)_2$·CB[8] exhibited relatively stabled at different concentrations (Figure S19a). A notable increase in the emission intensity ratio of fluorescence to phosphorescence (I_{387}/I_{500}) was observed when the concentration of $(BPBA)_2$·CB[8] was less than 16.7 μg/mL (Figure S19b). Consequently, the $(BPBA)_2$·CB[8] concentration was determined to be 16.7 μg/mL. Figure S20 showed that the emission change reached equilibrium in 15 seconds after the addition of PEA, indicating that $(BPBA)_2$·CB[8] can rapidly respond to PEA. To obtain the standard deviation, each sample was subjected to three parallel tests. Upon the gradual addition of PEA, the emission intensity at 387 nm increased while the emission at 500 nm decreased (Figure 5a). Additionally, the emission color changed from green to dark blue, and the corresponding CIE coordinates shifted from (0.1863, 0.3646) to (0.1647, 0.0907) (see Figure 5c).

Specifically, the emission intensity ratio of I_{387}/I_{500} demonstrated linearity as a function of PEA concentration in the range of 4-48 μM (Figure 5b). This indicates that $(BPBA)_2$·CB[8] can function as self-reference luminescent PEA sensor, with a limit of detection (LOD) as low as 27.5 nM, calculated according to the $3\sigma/k$ method.[42] To be noticed, this is the first fluorescence-phosphorescence dual-signal output ratiometric probe for quantitatively detecting low concentration PEA in aqueous solution. Meanwhile, this probe exhibits a higher sensitivity compared with many reported methods, including liquid chromatography and electrochemical method, and specifically, the LOD value is two orders of magnitude lower than reported colorimetric fluorescence sensors (Table S3).[7,43-48]

As urine testing is an important means of detecting drugs and their metabolites, we simulated the detection behavior of $(BPBA)_2$·CB[8] toward PEA in urine (Figure 5d, e). The photoluminescence spectra of $(BPBA)_2$·CB[8] showed no significant change in the presence of the main components of urine (KCl, Na_2SO_4, NH_4Cl, NaCl, creatinine, urea, uric acid, citric acid, glucose). Importantly, the addition of interfering substances did not cause any obvious change in I_{387}/I_{500}, demonstrating that $(BPBA)_2$·CB[8] remained high selectivity to PEA in the presence of major components of urine. In addition, as illustrated in Figure S21, the impact of common amino acids, cations, and anions on the spectrum of $(BPBA)_2$·CB[8] can be ignored. Subsequently, the photoluminescence response behavior of $(BPBA)_2$·CB[8] toward PEA in real urine was evaluated by a spiked recovery method (Supporting Information). As shown in Figure S18a, in the presence of PEA, the photoluminescence spectra of $(BPBA)_2$·CB[8] showed the similar change to that in water, with color change from green to dark blue was also observed (Figure S22a). The concentration-dependent linearity of I_{387}/I_{500} was observed for PEA concentration ranging from 4-48 μM, with a LOD of 29.8 nM (Figure S22b). In the control experiment without PEA, the photoluminescence spectra of $(BPBA)_2$·CB[8] in urine exhibited no discernible difference from that observed in water (Figure S23). As shown in Table S4, the standard addition recoveries of the spiked urine samples ranged from 97.0 to 102.0%, as determined by the obtained calibration curves. These results suggest that $(BPBA)_2$·CB[8] is a promising ratiometric photoluminescence probe for monitoring of PEA in urine with high sensitivity, accuracy and satisfactory selectivity. As a proof of concept, $(BPBA)_2$·CB[8] was made into a LFIA strip. As illustrated in Figure 5f, for a negative assay without PEA, the strip displayed green color under a 302 nm UV lamp. In contrast, an increase in PEA concentration resulted in a color change from green to blue, indicating the rapid on-site visual detection capability of $(BPBA)_2$·CB[8] toward PEA.

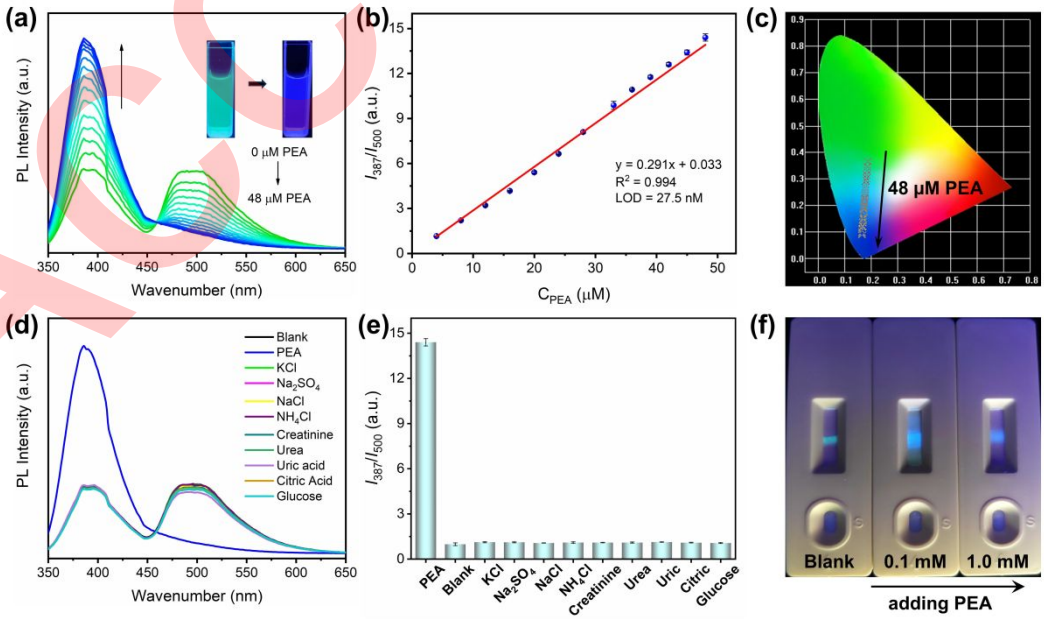

Figure 5 The ratiometric photoluminescent detection behavior of $(BPBA)_2$·CB[8] toward PEA. (a) The photoluminescence spectra (λ_{ex} = 345 nm) of $(BPBA)_2$·CB[8] suspension (16.7 μg/mL) upon the addition of PEA in water (0-48 μM). Inset: The photos of $(BPBA)_2$·CB[8] suspension before and after the addition of PEA under a 302 nm UV lamp. (b) Linear plot of I_{387}/I_{500} versus the concentration of PEA (4-48 μM). (c) The corresponding CIE coordinates of

(BPBA)$_2$·CB[8] suspension with the addition of PEA. The photoluminescence spectra (d) and I_{387}/I_{500} (e) of (BPBA)$_2$·CB[8] upon the addition of PEA and other interfering substances (48 μM). (f) The photos of LFIA strips at different concentration of PEA under a 302 nm UV lamp.

3.6 Detection mechanism investigation

To further investigate the photoluminescent detection mechanism, a series of tests were conducted. As mentioned above, PEA almost completely quenched the RTP of (BPBA)$_2$·CB[8] (Figure S24), and the photoluminescence spectrum recovered to a state similar to that of free BPBA (Figure S25). We therefore speculated that BPBA was squeezed out of the CB[8] cavity by PEA. ^{1}H NMR experiments were performed to verify the competitive binding behavior between PEA and BPBA□CB[8]. The methylene protons of free PEA (H_a and H_b) showed downfield shifts after adding CB[8], while the aromatic protons (H_c-H_e) showed slight upfield shifts (Figure 6b), indicating that the aromatic ring of PEA was located inside the cavity of CB[8], while the alkyl link of PEA was located outside the CB[8] port. This result shows that CB[8] also can encapsulate PEA to form host-guest complex. Upon the addition of PEA to BPBA□CB[8], the protons of BPBA (H_1-H_3) shifted to downfield (Δδ = 1.21 ppm, 1.12 ppm and 0.50 ppm, respectively), while H_6 and H_7 shifted to upfield (Δδ = 0.29 ppm and 0.08 ppm, respectively) (Figure 6b), indicating that the BPBA was squeezed out of the CB[8] cavity. Interestingly, the protons of BPBA (H_6 and H_7) cannot fully recover to the original state of free BPBA, whereas all the protons of PEA (H_a-H_e) showed downfield movements when compared with those of PEA□CB[8] (Figure 6b), which may be attributed to the formation of hydrogen bonds between the amino group of PEA and the carboxyl group of BPBA. To verify our hypothesis, we tested the ^{1}H NMR of the PEA and BPBA mixture (BPBA-PEA), the protons of BPBA (H_6 and H_7) shifted to upfield (Δδ = 0.11 ppm and 0.03 ppm, respectively), while all the protons of PEA (H_a-H_e) showed downfield movements (Δδ = 0.16 ppm, 0.10 ppm, 0.04 ppm, 0.04 ppm and 0.04 ppm, respectively) (Figure S26), confirming the existence of hydrogen bonds between PEA and BPBA. Thus, the chemical shift observed in the mixture of PEA and BPBA□CB[8] results from PEA displacing BPBA from the cavity of CB[8] and forming hydrogen bonds with BPBA. In the ESI-MS spectrum of BPBA□CB[8] with the addition of 0.5 eq. PEA, a dominant peak at 786.2954 was observed, which corresponds to the theoretical value of $[2PEA + CB[8] + 2H]^{2+}$ (786.2928) (Figure 6c). In addition, a weak peak at 909.2622 was also observed corresponded to the theoretical value of $[BPBA + PEA + CB[8] + H - Cl]^{2+}$ (909.2584), and its intensity was further weakened upon the addition of 1.0 eq. PEA, demonstrating that PEA squeezed BPBA out of the CB[8] cavity to form a new 1:2 host-guest complex (PEA□CB[8]) (Figure 6a). Furthermore, the binding constants of PEA□CB[8] obtained from UV-vis titration are $K_1 = 7.34 \times 10^5$ M^{-1} and $K_2 = 2.12 \times 10^4$ M^{-1}, in which K_1 of PEA□CB[8] is higher than K_1 and K_2 of BPBA□CB[8] (2.03×10^5 M^{-1} and 3.23×10^4 M^{-1}, respectively). The *ternary* equilibrium binding constant of PEA□CB[8] (1.56×10^{10} M^{-2}) is higher than that of BPBA□CB[8] (6.56×10^9 M^{-2}), which explains why PEA can compete BPBA out of the cavity of CB[8] (Figure 6d and Figure S27a). Importantly, the UV-vis absorption spectra indicated a gradual increase in the absorption peak of BPBA□CB[8] upon the addition of 0-1.0 eq. PEA, accompanied by a blue shift from 312 to 310 nm (Figure S27b), further indicating the dissociation of BPBA□CB[8]. All of the results demonstrate that (BPBA)$_2$·CB[8] was dissociated in the presence of PEA, resulting in the quenching of RTP and recovery of fluorescence.

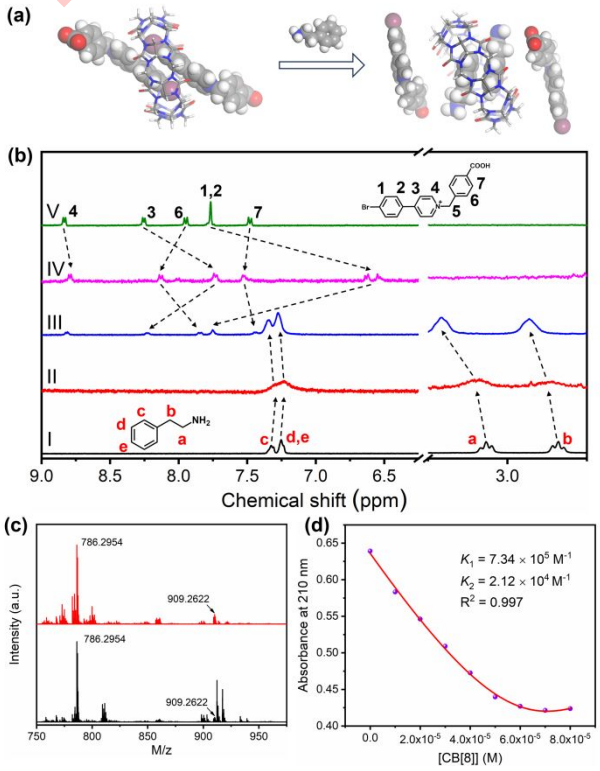

Figure 6 The detection mechanism. (a) Schematic illustration of the detection behavior of (BPBA)$_2$·CB[8] to PEA. (b) The ^{1}H NMR of PEA (I),

PEA□CB[8] (II), BPBA□CB[8] before (IV) and after (III) the addition of PEA, and free BPBA (V) ([PEA] = [BPBA] = 2[CB[8]] = 1.2 mM) (D_2O, 400 MHz, 298 K). (c) The ESI-MS spectra of the BPBA□CB[8] with the addition of 0.5 eq. PEA (top, [BPBA]:[CB[8]]:[PEA] = 2:1:1) and 1.0 eq. PEA (bottom, [BPBA]:[CB[8]]:[PEA] = 2:1:2). (d) The nonlinear least-squares analyses of the UV absorbance changes with addition 0-0.8 eq. CB[8] to calculate the association constants between PEA and CB[8] ([PEA]= 0.1 mM).

4 Conclusions

In summary, we realized ultrastrong and high-efficiency room-temperature phosphorescence in crystalline host-guest complex formed by self-assembly of 4-(4-bromophenyl)-pyridinium derivatives and CB[8] in water. Single-crystal structure analysis revealed that the rigid environment and multiple weak interactions in crystal effectively promoted the ISC process, reduced the quenching of environmental conditions and stabilize the triple exciton, resulting in enhanced green RTP. In addition, the obtained crystalline host-guest complex demonstrated the ability of rapid identification and sensitive ratiometric luminescent detection of PEA with a LOD of 27.5 nM, and allow for instant visual detection. This work will not only contribute to a more in-depth understanding of the mechanism of CB[8]-mediated RTP, but will also extend the range of applications of RTP.

Acknowledgments This work was financially supported by the National Natural Science Foundation of China (22171069 and 21871075), the Educational Committee of Hebei Province (JZX2024012) and the Tianjin Natural Science Foundation (23JCYBJC00800).

Conflict of interest The authors declare that they have no conflict of interest.

Supporting information The supporting information is available online at http://chem.scichina.com and http://link.springer.com/journal/11426. The supporting materials are published as submitted, without typesetting or editing. The responsibility for scientific accuracy and content remains entirely with the authors.

1 Liu K, Shang C, Wang Z, Qi Y, Miao R, Liu K, Liu T, Fang Y. *Nat. Commun.*, 2018, 9: 1695
2 Basilicata P, Pieri M, Settembre V, Galdiero A, Della Casa E, Acampora A, Miraglia N. *Anal. Chem.*, 2011, 83: 8566-8574
3 Zhu Y, Zhu Y, Xu J. *Chin. Chem. Lett.*, 2023, 34: 107391
4 Marcobal A, Polo MC, Martín-Álvarez PJ, Moreno-Arribas MV. *Food Res. Inter.*, 2005, 38: 387-394
5 Borgul P, Sobczak K, Rudnicki K, Glazer P, Pawlak P, Trynda A, Skrzypek S, Poltorak L. *Electrochim. Acta*, 2022, 402: 139553
6 Liu K-K, Meng Z, Fang Y, Jiang H-L. *eScience*, 2023, 3: 100133
7 Liu Y, Dan W, Yan B. *J. Mater. Chem. A*, 2024, 12: 1498-1505
8 Feng T, Ye Y, Liu X, Cui H, Li Z, Zhang Y, Liang B, Li H, Chen B. *Angew. Chem. Inter. Ed.*, 2020, 48: 21752-21757
9 Liu X, Ye Y, He X, Niu Q, Chen B, Li Z. *Angew. Chem. Inter. Ed.*, 2024, 63: e202400195
10 Li L, Zhou Z, Huang F, Peng S, Huang Y, Wang G, Li X, Chen F-F, Yang C, Li X-X, Yu Y. *J. Rare Earths*, 2023, 41: 42-50
11 Jin H, Jiang X, Sun Z, Gui R. *Coord. Chem. Rev.*, 2021, 431: 213694
12 Dong X-Y, Si Y, Yang J-S, Zhang C, Han Z, Luo P, Wang Z-Y, Zang S-Q, Mak TC. *Nat. Commun.*, 2020, 11: 3678
13 Zhang KY, Zhang J, Liu Y, Liu S, Zhang P, Zhao Q, Tang Y, Huang W. *Chem. Sci.*, 2015, 6: 301-307
14 Li Z, Liu X, Wang G, Li B, Chen H, Li H, Zhao Y. *Nat. Commun.*, 2021, 12: 1363
15 Li K, Chen Y, Wang J, Yang C. *Coord. Chem. Rev.*, 2021, 433: 213755
16 Shimizu M, Sakurai T. *ChemPlusChem*, 2021, 86: 446-459
17 Bi X, Shi Y, Peng T, Yue S, Wang F, Zheng L, Cao QE. *Adv. Funct. Mater.*, 2021, 31: 2101312
18 Dai W, Niu X, Wu X, Ren Y, Zhang Y, Li G, Su H, Lei Y, Xiao J, Shi J. *Angew. Chem. Inter. Ed.*, 2022, 61: e202200236
19 Kabe R, Notsuka N, Yoshida K, Adachi C. *Adv. Mater.*, 2016, 28: 655-660
20 Fan Y, Li Q, Li Z. *Sci. China Chem.*, 2023, 66: 2930-2940
21 Yang J, Fang M, Li Z. *Acc. Mater. Res.*, 2021, 2: 644-654
22 Sun H, Zhu L. *Aggregate*, 2023, 4: e253
23 Wu H. *Angew. Chem. Inter. Ed.*, 2019, 58: 4328-4333
24 Ma X-K, Liu Y. *Acc. Chem. Res.*, 2021, 54: 3403-3414
25 Nie F, Yan D. *Sci. China Chem.*, 2023, 66: 611-612
26 Xiong S, Xiong Y, Wang D, Pan Y, Chen K, Zhao Z, Wang D, Tang BZ. *Adv. Mater.*, 2023, 2301874
27 Wang D, Gong J, Xiong Y, Wu H, Zhao Z, Wang D, Tang BZ. *Adv. Funct. Mater.*, 2023, 33: 2208895
28 El-Naggar ME, Ullah S, Wageh S, Abu-Saied MA, Khattab TA, Alhashmialameer D, Abou Taleb M, Matter EA. *J. Rare Earths*, 2023, 41: 397-405
29 Zhang ZY, Xu WW, Xu WS, Niu J, Sun XH, Liu Y. *Angew. Chem. Inter. Ed.*, 2020, 59: 18748-18754
30 Yang Z, Xu C, Li W, Mao Z, Ge X, Huang Q, Deng H, Zhao J, Gu FL, Zhang Y. *Angew. Chem. Inter. Ed.*, 2020, 59: 17451-17455
31 Zhang Z-Y, Liu Y. *Chem. Sci.*, 2019, 10: 7773-7778
32 Xu WW, Chen Y, Lu YL, Qin YX, Zhang H, Xu X, Liu Y. *Angew. Chem. Inter. Ed.*, 2022, 61: e202115265
33 Nie H, Wei Z, Ni X-L, Liu Y. *Chem. Rev.*, 2022, 122: 9032-9077
34 Ma L, Ma X. *Sci. China Chem.*, 2023, 66: 304-314
35 Dai X-Y, Huo M, Liu Y. *Nat. Rev. Chem.*, 2023, 7: 854-874
36 Wang J, Huang Z, Ma X, Tian H. *Angew. Chem. Inter. Ed.*, 2020, 59: 9928-9933
37 Zhang Q-S, Zhang X-D, Zhuang J-Y, Pan M. *Aggregate*, 2024, 5: e456
38 Bai Q, Xia Y, Kang Y, Jiang Y, Hu J, Ma P, Tao Z, Xiao X. *Chem. Eng. J.*, 2023, 477: 146922
39 Xu C, Yin C, Wu W, Ma X. *Sci. China Chem.*, 2022, 65: 75-81
40 Zhang W, Luo Y, Liu C, Yang M-X, Gou J-X, Huang Y, Ni X-L, Tao Z, Xiao X. *ACS Appl. Mater. Interfaces*, 2022, 14: 51429-51437
41 Zhou W-L, Chen Y, Yu Q, Zhang H, Liu Z-X, Dai X-Y, Li J-J, Liu Y. *Nat. Commun.*, 2020, 11: 4655
42 Zheng Z, Yu H, Geng W-C, Hu X-Y, Wang Y-Y, Li Z, Wang Y, Guo D-S. *Nat. Commun.*, 2019, 10: 5762
43 Tanen JL, Lurie IS, Marginean I. *Forensic Chem.*, 2020, 21: 100281
44 Ta š ev K, Ivanova-Petropulos V, Stefova M. *Food Anal. Methods*, 2017, 10: 4038-4048
45 Ma S, Wang Y, Jiang L, Hu R, Luo Z, Li G. *Measurement Sci. Tech.*, 2021, 32: 115116
46 Allahverdiyeva S, Keskin E, Pınar PT, Yardım Y, Şentürk Z. *Electroanalysis*, 2019, 31: 2283-2289

47 Rosa-Gastaldo D, Scopano A, Zaramella M, Mancin F. *ACS Appl. Nano Mater.*, 2020, 3: 9616-9621
48 Hsu L-W, Lin Y-H, Guo J-Y, Chen C-F, Chou Y-J, Yeh Y-C. *ACS Appl. Bio Mater.*, 2020, 3: 5120-5125

Table of Contents graphic

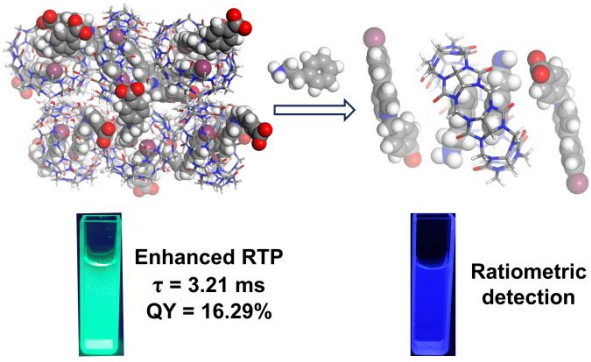

A 4-(4-bromophenyl)-pyridinium derivative and cucurbit[8]uril self-assemble in aqueous to form a crystalline 1:2 host-guest complex with ultralong RTP lifetime of 3.21 ms and RTP quantum yield of up to 16.29%, capable of rapid identification and sensitive fluorescence-phosphorescence ratiometric detection of psychoactive substance.

Supporting Information for

Ultrastrong room-temperature phosphorescence in cucurbit[8]uril-mediated crystalline supramolecules for ratiometric detection of phenethylamine

Qingyu Niu,[1+] Yingxiang Ye,[2+] Lingna Su,[1] Xu He,[1] Zhiqiang Li,[1,3]* and Yu Liu[4]*

[1]School of Chemical Engineering and Technology, Hebei University of Technology, GuangRong Dao 8, Hongqiao District, Tianjin 300130, P. R. China. *E-mail: zhiqiangli@hebut.edu.cn

[2]Fujian Provincial Key Laboratory of Polymer Materials, College of Chemistry and Materials Science, Fujian Normal University, Shangsan Road 8, Cangshan District, Fuzhou, Fujian 350007, China.

[3]Key Laboratory of Advanced Energy Materials Chemistry (Ministry of Education), Nankai University, Tianjin 300071, China

[4]College of Chemistry, State Key Laboratory of Elemento-Organic Chemistry, Nankai University, Weijin Road 94, Nankai District, Tianjin 300071, P. R. China. *E-mail: yuliu@nankai.edu.cn

Niu QYand Ye YX contributed equally to this work.

https://www.sciengine.com/doi/10.1007/s11426-024-2410-x
http://chem.scichina.com/english

Experiment Section

Characterization methods

Crystal was measured on a Bruker D8 VENTURE MetalJet PHOTON II diffractometer. The crystal was kept at 150 K during data collection. Using Olex2, the structure was solved with the SHELXT structure solution program using Intrinsic Phasing and refined with the SHELXL refinement package using Least Squares minimization, and the crystal data of $(BPBA)_2$·CB[8] is given in Table S1. The FTIR data come from the Bruker Vector 22 spectrometer, and the measurement range is 4000-400 cm^{-1}. The ^1H NMR, 2D ROESY and ^{13}C NMR spectra were recorded by the Bruker 400 instrument. The liquid chromatography-mass spectrometry (LC-MS) was obtained with Compact Bruker Scientific Instrument. The electrospray ionization mass spectroscopy (ESI-MS) was obtained with Thermo Scientific QE plus. The experimental data of powder X-ray diffraction (PXRD) were collected on Rigaku X-ray diffractometer (Smartlab). Thermogravimetric analysis (TGA) was carried out under an N_2 atmosphere from room temperature to 800 °C using a Shimadzu TGA-50 analyzer at a heating rate of 10 °C/min. Photoluminescence spectra, lifetime and quantum efficiency were obtained on FLS1000 (Edinburg Instruments, Livingstone, UK). UV-vis absorbance spectra were record on an Agilent Carry 100 UV-vis spectrophotometer in a conventional rectangular quartz cell (10 × 10 × 45 mm) at 25 °C. Scanning electron microscopy (SEM) image was obtained with a Quanta 450 FEG scanning electron microscope.

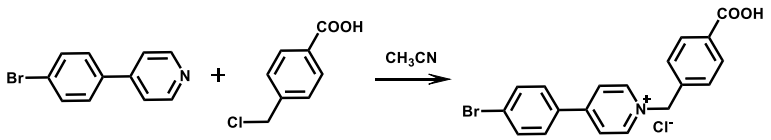

Scheme S1. The synthetic route of compound BPBA.

Synthesis of single crystal $(BPBA)_2$·CB[8]

Colorless rod-like single crystal of $(BPBA)_2$·CB[8] was obtained by allowing a

saturated solution of BPBA⊂CB[8] to stand for a week at room temperature ([BPBA] = 2[CB[8]] = 0.167 mM).

Preparation of $(BPBA)_2$·CB[8] suspension

The $(BPBA)_2$·CB[8] crystal was dispersed in water and then subjected to ultrasound to produce a series of water suspensions with varying concentrations (500, 50.0, 33.4, 16.7, 8.4, 4.2 μg/mL).

Fabrication of lateral flow immunoassay (LFIA) strip

$(BPBA)_2$·CB[8] suspension (500 μg/mL) was dispensed into the nitrocellulose membrane and dried at 37 °C (10 μg/cm). Next, the sample pad, conjugate pad, nitrocellulose membrane and absorbent pad were assembled to a polystyrene backing card with 2 mm overlap. The card was cut into 4 mm-wide strips, which were stored in a desiccator at room temperature.

Pretreatment of real urine samples

The real urine was subjected to centrifugation, dilution, and filtration through a nylon membrane with a diameter of 0.22 μm, with the objective of eliminating insoluble particles. Subsequently, emission spectra were obtained by adding varying quantities of PEA to the treated urine samples.

Theoretical calculation

The photophysical parameters are obtained according to the following equations.[1]

$$k_{isc} = \frac{\phi_{Phos}}{\tau_{Fluo}}$$

$$k_{nr}^{Phos} = \frac{1 - \phi_{Phos}}{\tau_{phos}}$$

$$k_{r}^{Phos} = \frac{\phi_{Phos}}{\tau_{phos}}$$

https://www.sciengine.com/doi/10.1007/s11426-024-2410-x
http://chem.scichina.com/english

$$\phi_{Phos} = \frac{k_r^{Phos} * \phi_{isc}}{k_r^{Phos} + k_{nr}^{Phos}}$$

$$\tau_{Phos} = \frac{1}{k_r^{Phos} + k_{nr}^{Phos}}$$

Where k_{isc} is the intersystem crossing rate constant, k_r^{phos} is the radiative decay rate constant of phosphorescence, k_{nr}^{phos} is the nonradiative decay rate constant of phosphorescence, Φ_{phos} is the intersystem crossing process quantum yield.

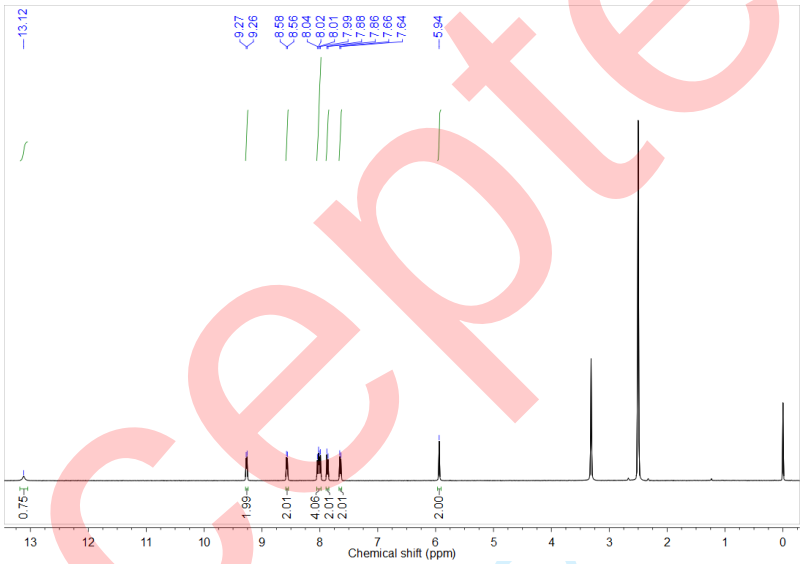

Figure S1. ^{1}H NMR spectrum of compound BPBA (DMSO-d_6, 400 MHz, 298 K).

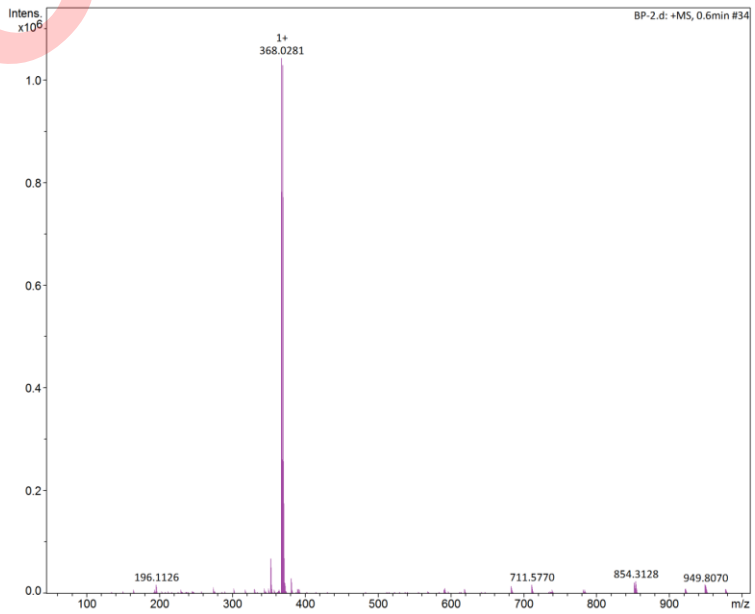

Figure S2. LC-MS spectrum of compound BPBA.

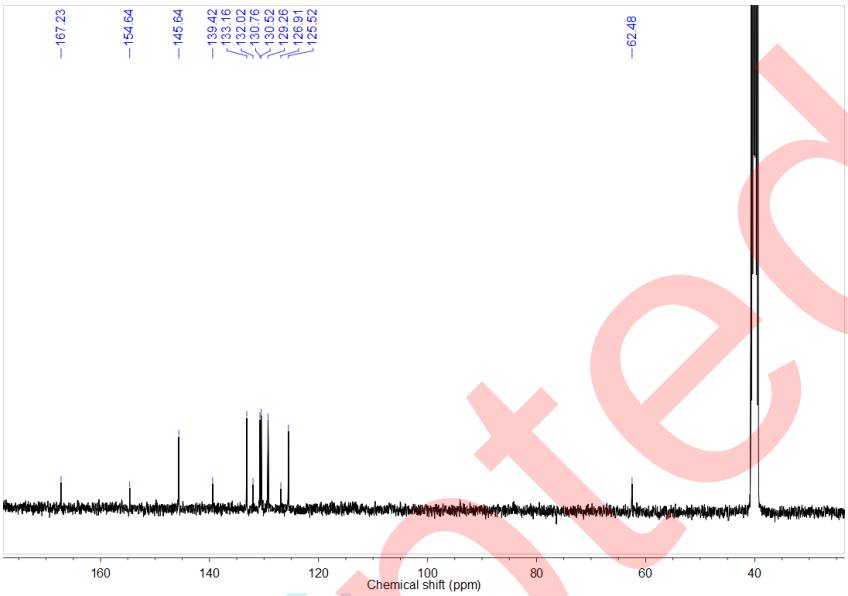

Figure S3. ^{13}C NMR spectrum of compound BPBA (DMSO-d_6, 100 MHz, 298 K).

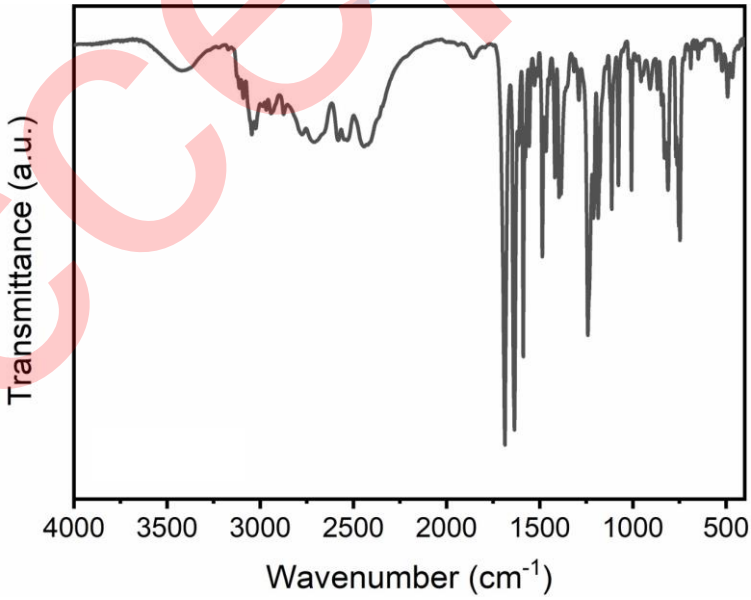

Figure S4. FTIR spectrum of compound BPBA.

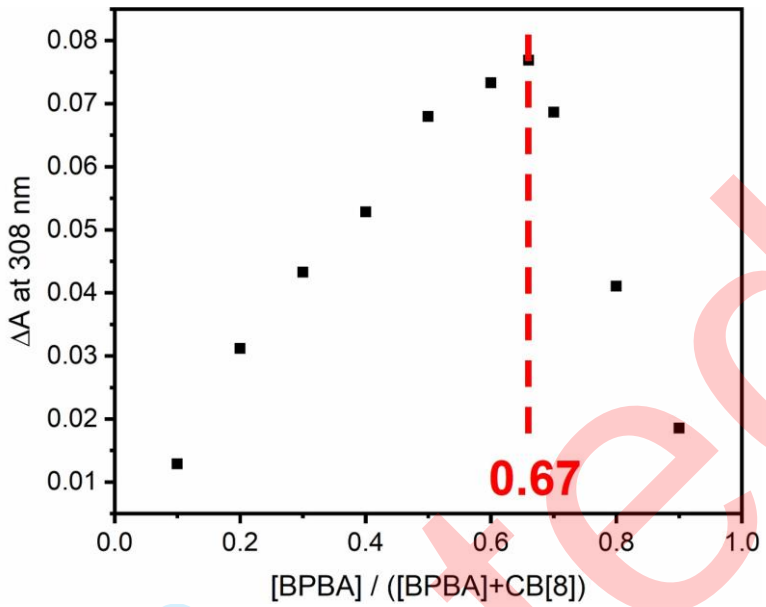

Figure S5. Job's plot for the complexation between BPBA and CB[8] (total concentration 20 μM).

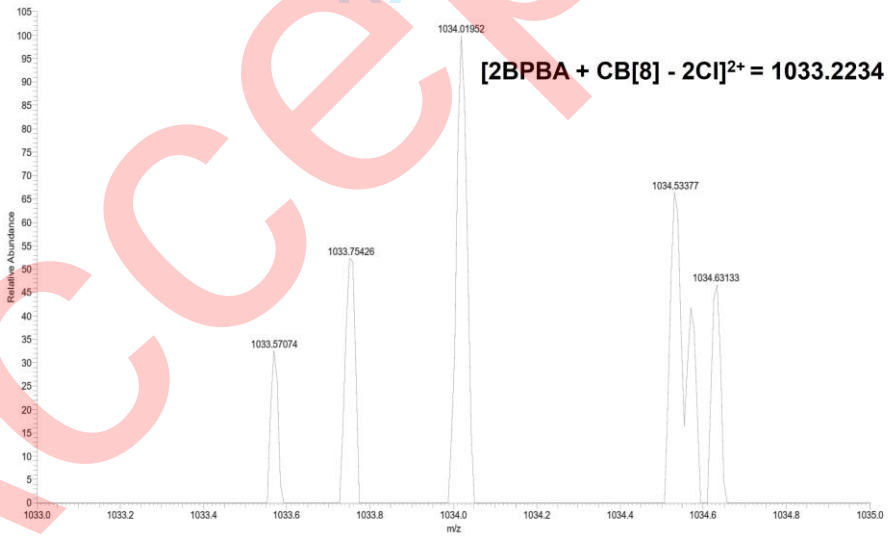

Figure S6. ESI-MS spectrum of BPBA⊂CB[8].

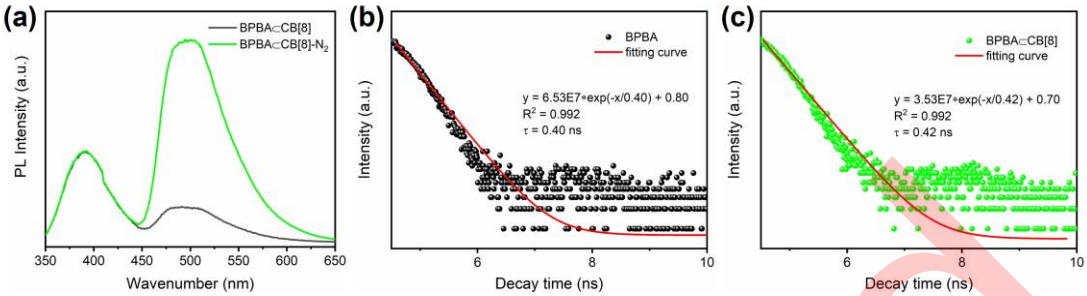

Figure S7. (a) The photoluminescence spectra of BPBA⊂CB[8] under air condition and N_2 atmosphere (λ_{ex}= 330 nm, [BPBA] = 2[CB[8]] = 20 μM). The lifetime of (b) free BPBA and (c) the BPBA⊂CB[8] complex in aqueous solution measured at 387 nm ([BPBA] = 2[CB[8]] = 20 μM). The y-axis of Figure S7b, c is presented in a logarithmic scale.

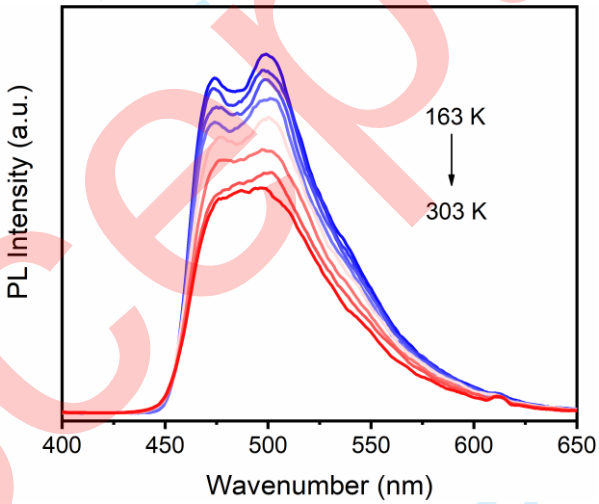

Figure S8. The temperature-dependent delayed spectra of BPBA⊂CB[8] (λ_{ex}= 330 nm).

https://www.sciengine.com/doi/10.1007/s11426-024-2410-x
http://chem.scichina.com/english

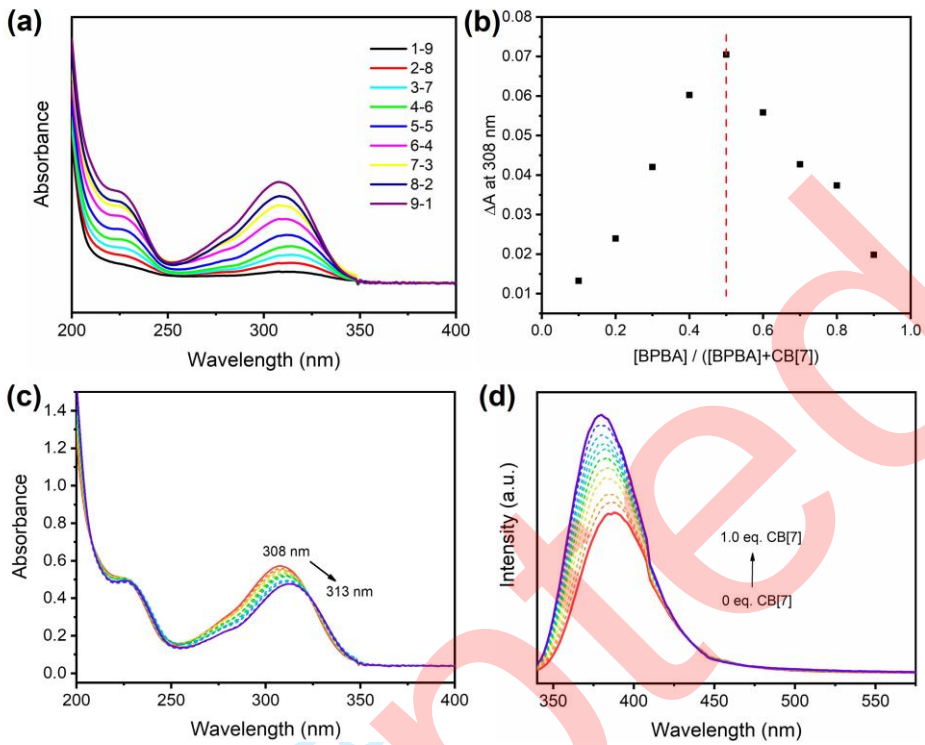

Figure S9. UV-vis absorption spectra (a) and Job's plot (b) for the complexation between BPBA and CB[7] (total concentration 20 μM). UV-vis absorption spectra (c) and photoluminescence emission spectra (d) of BPBA (20 μM) with different ratio of CB[7] (0-1.0 eq) in H_2O at 298 K (λ_{ex} = 330 nm).

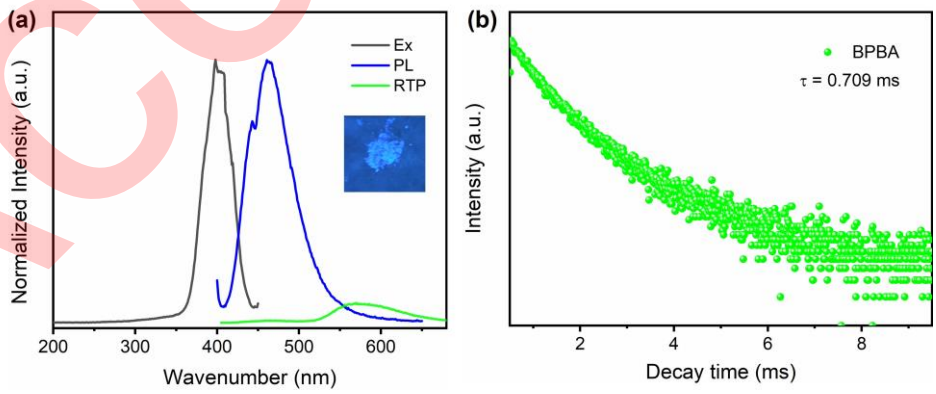

Figure S10. (a) Excitation, photoluminescence (λ_{ex}= 398 nm), RTP spectra and (b) RTP decay curve (delayed by 0.5 ms) of solid-state BPBA. Inset: the photo of BPBA powder under a 365 nm UV lamp.

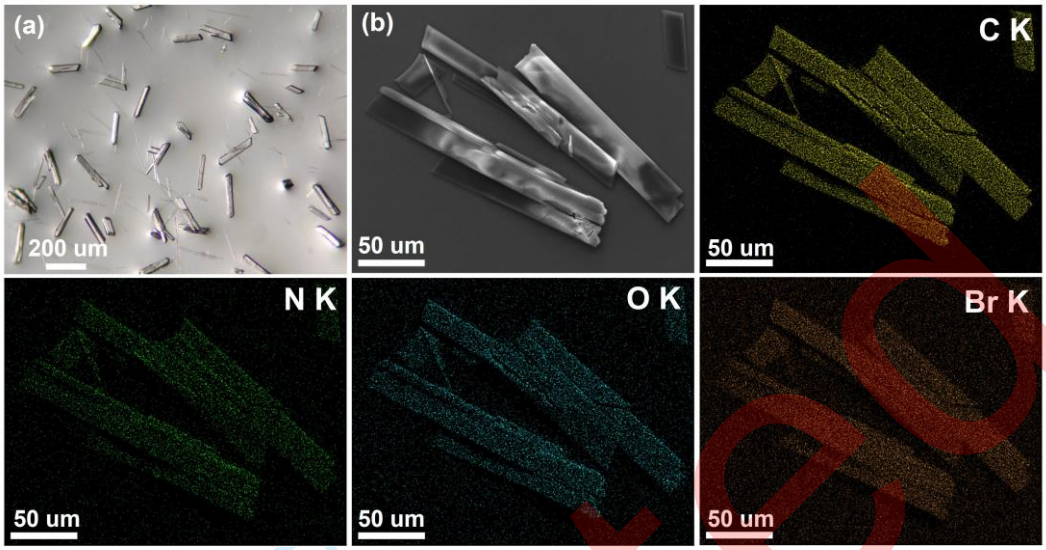

Figure S11. Optical microscope image (a), SEM image (b) and EDS mapping of the $(BPBA)_2 \cdot CB[8]$ crystal.

https://www.sciengine.com/doi/10.1007/s11426-024-2410-x
http://chem.scichina.com/english

Table S1. Crystal data and structure refinement parameters for $(BPBA)_2$·CB[8].

Compound	**$(BPBA)_2$·CB[8]**
CCDC	2359823
Empirical formula	$C_{172}H_{213}Br_4N_{68}O_{70.5}$
Formula weight	4680.73
Temperature (K)	150.00
Crystal system	Triclinic
Space group	*P*-1
a (Å)	17.6926(16)
b (Å)	23.526(2)
c (Å)	27.594(2)
α (°)	96.294(3)
β (°)	103.719(3)
γ (°)	109.792(3)
Volume ($Å^3$)	10269.5(16)
Z	2
Density (g/cm^3)	1.514
Absorption coefficient (mm^{-1})	1.216
F(000)	4850.0
Crystal size (mm^3)	0.12 × 0.1 × 0.08
Radiation	Ga-Kα (λ = 1.34139 Å)
Theta range for data collection (°)	4.83 to 107.814
Index ranges	$-21 \le h \le 20$, $-28 \le k \le 28$, $-33 \le l \le 32$
Reflections collected	130784
Independent reflections	37530 [R_{int} = 0.0788, R_{sigma} = 0.0760]
Data/restraints/parameters	37530/2551/2914
Goodness-of-fit on F^2	1.068
Final R indexes [I>=2σ (I)][(a)]	R_1 = 0.0750, wR_2 = 0.2063
Final R indexes [all data][(a)]	R_1 = 0.1200, wR_2 = 0.2367

(*a*) $R_1 = \Sigma||F_O| - |F_C|| / \Sigma|F_O|; wR_2 = [\Sigma w(|F_O|^2 - |F_C|^2)^2 / \Sigma w(F_O^2)^2]^{1/2}$

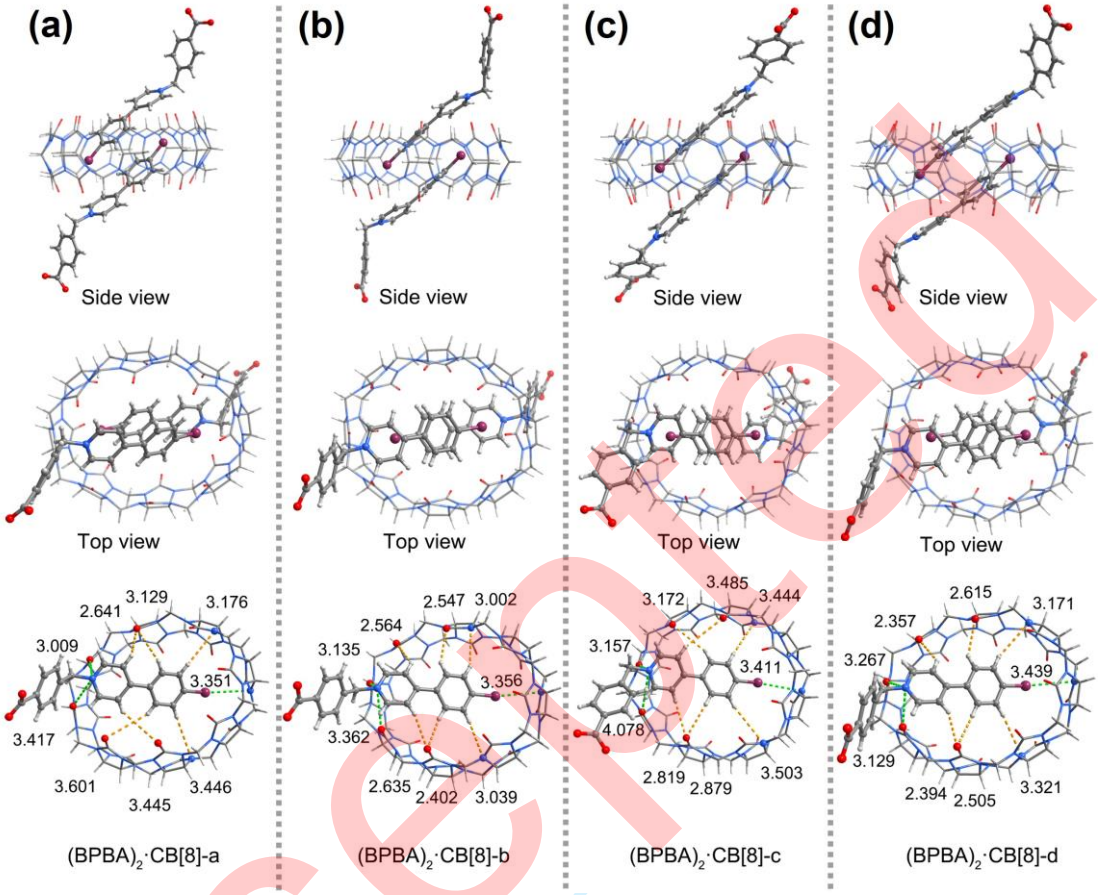

Figure S12. Crystal structure of $(BPBA)_2$·CB[8]. (a-d) Side view, top view and the host-guest interactions of $(BPBA)_2$·CB[8]-a, $(BPBA)_2$·CB[8]-b, $(BPBA)_2$·CB[8]-c, and $(BPBA)_2$·CB[8]-d, respectively, the unit of distance is Å.

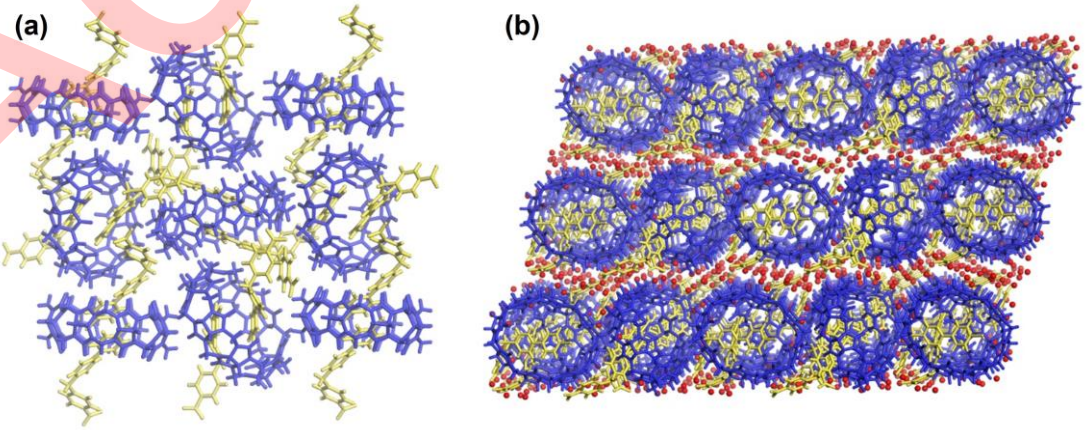

Figure S13. (a, b) Two-dimensional and three-dimensional molecular packing structures of $(BPBA)_2$·CB[8].

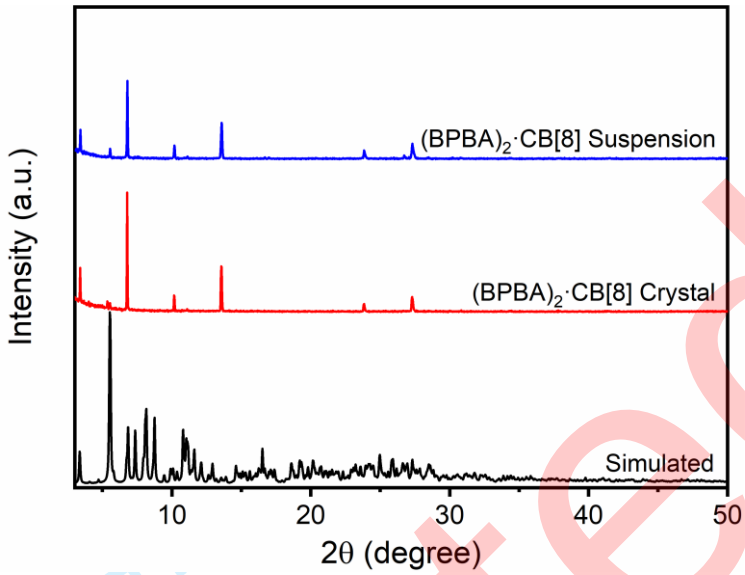

Figure S14. The PXRD patterns of the simulated single crystal $(BPBA)_2$·CB[8], experimental $(BPBA)_2$·CB[8] crystal and $(BPBA)_2$·CB[8] suspension.

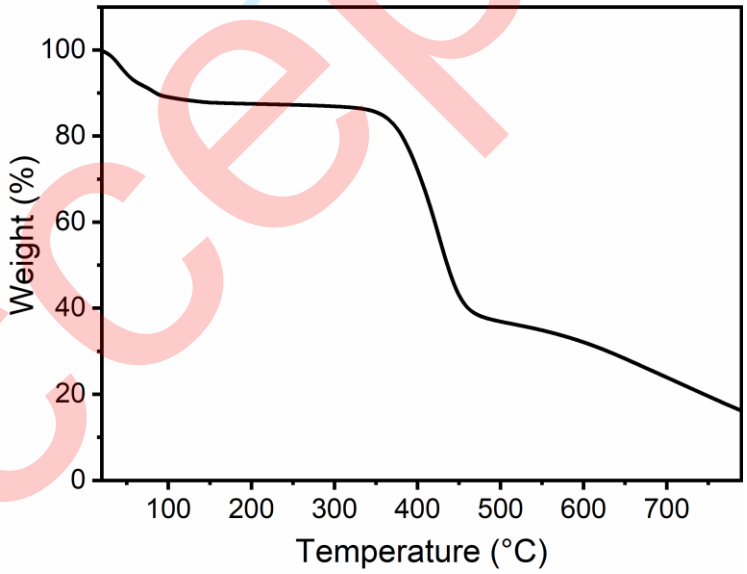

Figure S15. The TGA curve of $(BPBA)_2$·CB[8].

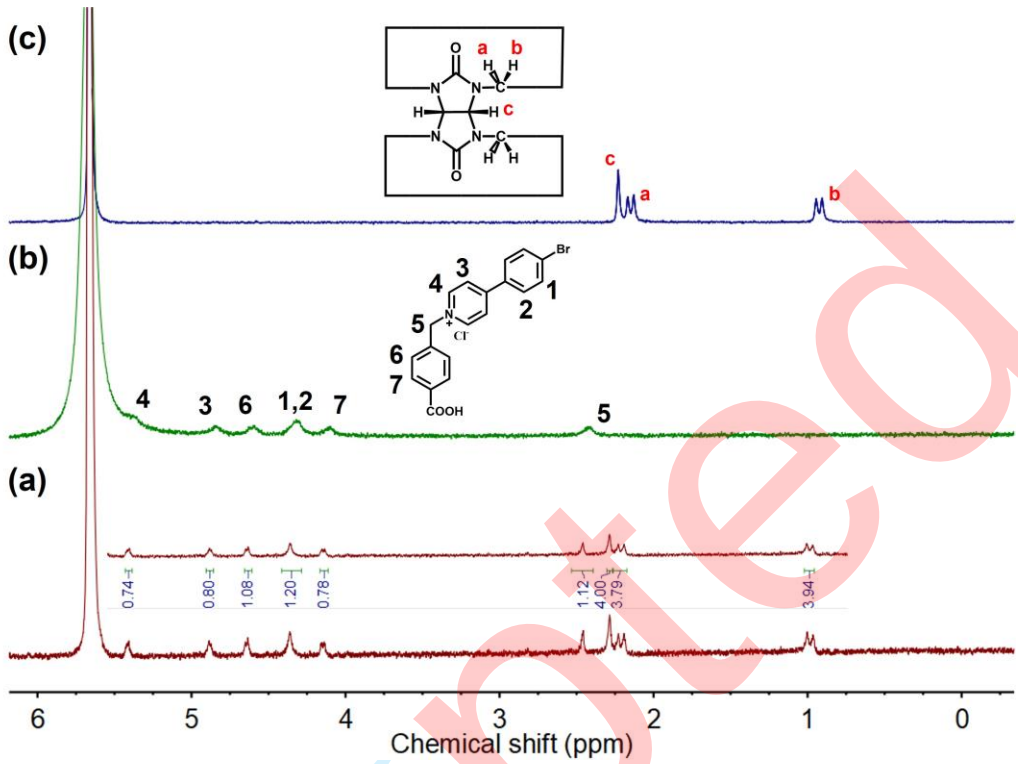

Figure S16. ^{1}H NMR of CB[8], BPBA and acid-digested $(BPBA)_2$·CB[8] (DCl in D_2O, 30 wt%, 400 MHz, 298 K).

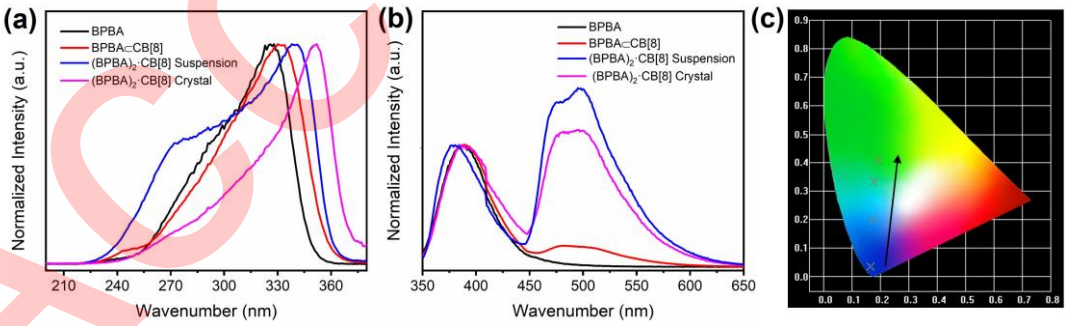

Figure S17. The excitation (a) and photoluminescent spectra (b) of BPBA, BPBA⊂CB[8], $(BPBA)_2$·CB[8] suspension and $(BPBA)_2$·CB[8] crystal, and (c) the corresponding CIE coordinates.

https://www.sciengine.com/doi/10.1007/s11426-024-2410-x
http://chem.scichina.com/english

Table S2. CB[8] confined aqueous RTP lifetime and Quantum yields in this work and previous reports.[1-18]

Guest	Name	τ_{RTP} (ms)	QY_{RTP} (%)	Reference
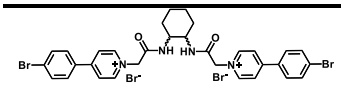	G⊂CB[8]	0.770	8.40	[2]
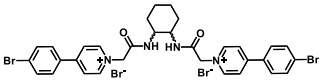	CB[8]/AHBP	0.489	4.00	[3]
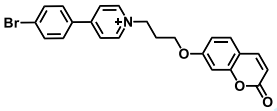	G⊂CB[8]	0.271	5.10	[4]
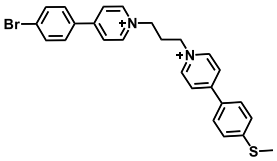	1/CB[8]	0.133	12.1	[5]
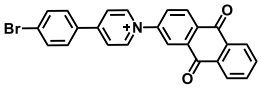	AQPY⊂CB[8]	0.377	1.53	[6]
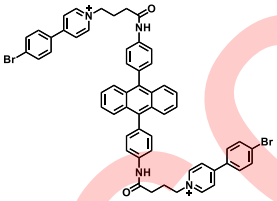	CB[8]/BPA	0.133	0.78	[7]
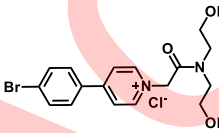	DA-PY/CB[8]	0.419	2.73	[8]
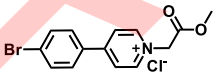	MA-PY/CB[8]	0.370	1.70	[8]
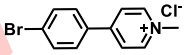	PY/CB[8]	0.264	1.14	[8]
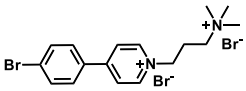	BPTN⊂CB[8]	0.602	2.10	[9]
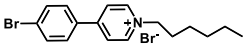	6C/CB[8]	1.26	3.47	[10]
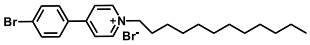	12C/CB[8]	0.700	2.74	[10]

https://www.sciengine.com/doi/10.1007/s11426-024-2410-x
http://chem.scichina.com/english

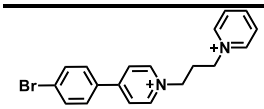	BPPY⊂CB[8]	0.377	2.80	[11]
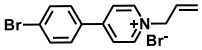	CB[8]/ABP	0.900	2.57	[12]
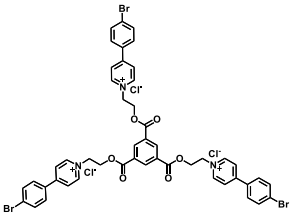	CB[8]-TBP	0.437	5.20	[13]
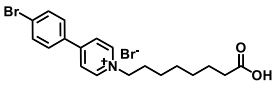	Q[8]-BPCOOH	0.530	4.94	[14]
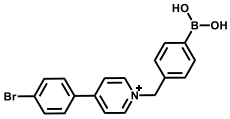	BH-PY/CB[8]	0.308	2.28	[15]
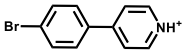	2-CB[8]	0.340	10.2	[16]
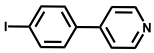	3-CB[8]	0.560	8.9	[16]
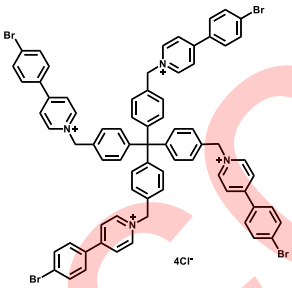	TBBP-CB[8]	0.451	2.30	[17]
	G⊂CB[8]	0.450	1.13	[18]
	G⊂CB[8]@PSS	2.39	13.16	[18]
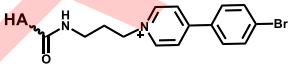	CB[8]/HA-BrBP	4.33	7.58	[1]
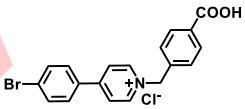	$(BPBA)_2$·CB[8] suspension	2.03	14.72	This work
	$(BPBA)_2$·CB[8] crystal	3.21	16.29	

https://www.sciengine.com/doi/10.1007/s11426-024-2410-x
http://chem.scichina.com/english

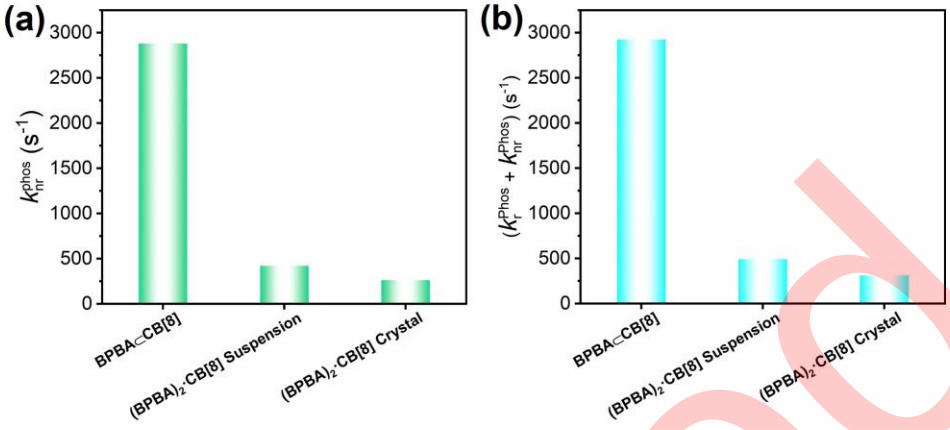

Figure S18. The photophysical parameters of different samples.

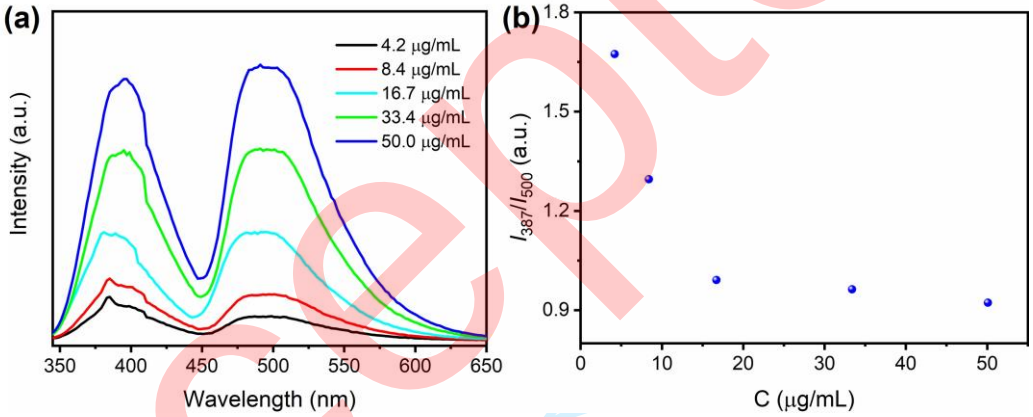

Figure S19. The photoluminescence spectra (λ_{ex} = 345 nm) and corresponding emission intensity ratio of I_{387}/I_{500} of (BPBA)$_2$·CB[8] at different concentrations.

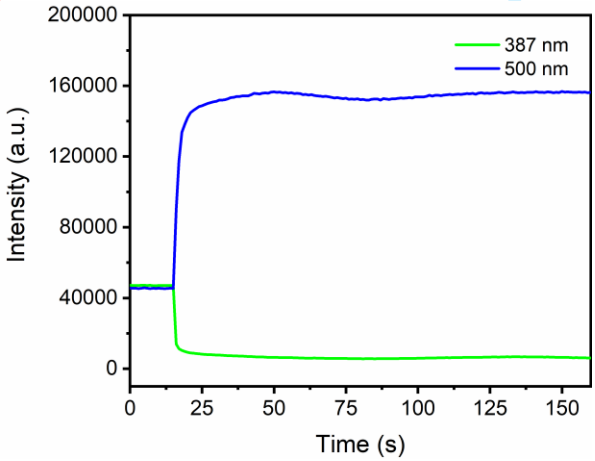

Figure S20. The photoluminescent intensity (I_{387} and I_{500}) of (BPBA)$_2$·CB[8] after the addition of 48 μM PEA at different time intervals.

https://www.sciengine.com/doi/10.1007/s11426-024-2410-x
http://chem.scichina.com/english

Table S3. Comparison of this work with other PEA-type drugs and their analogues sensors.

Analytical method	Linear range	LOD	Reference
Vacuum ultraviolet	6.25-200 μg·mL^{-1}	17.6 μM	[36]
Liquid Chromatography	0.50-30.0 μg·L^{-1}	8.25 nM	[37]
Electrochemical	5-100 μM	3.2 μM	[4]
Electrochemical	10^{-7}-10^{-2} M	1 μM	[38]
Electrochemical	3.0×10^{-5}-6.1×10^{-4} M	10.7 μM	[39]
colorimetric sensing	5-550 μM	3 μM	[40]
Fluorescence	5-50 μM	1.05 μM	[41]
Fluorescence	5×10^{-6}-10^{-3} M	2.56 μM	[6]
Ratiometric luminescence	1-48 μM	27.5 nM	This work

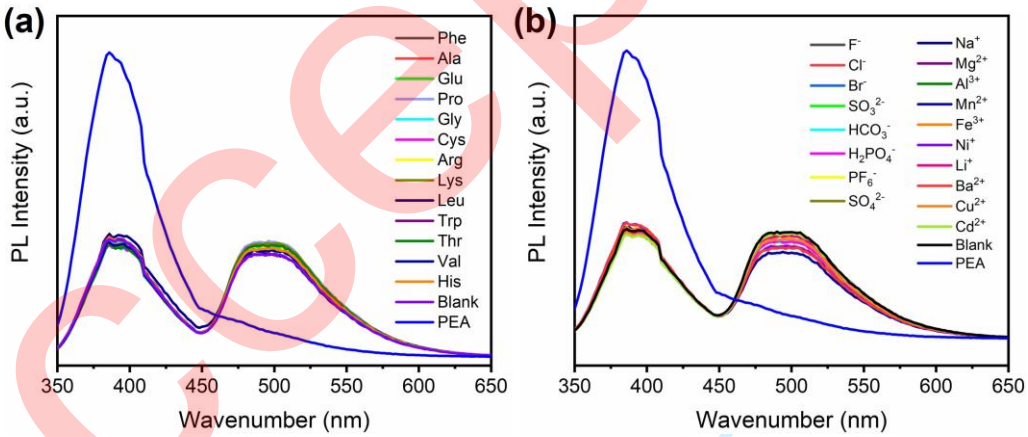

Figure S21. The photoluminescence spectra (λ_{ex} = 345 nm) of the $(BPBA)_2$·CB[8] in the presence of PEA and other interfering substances.

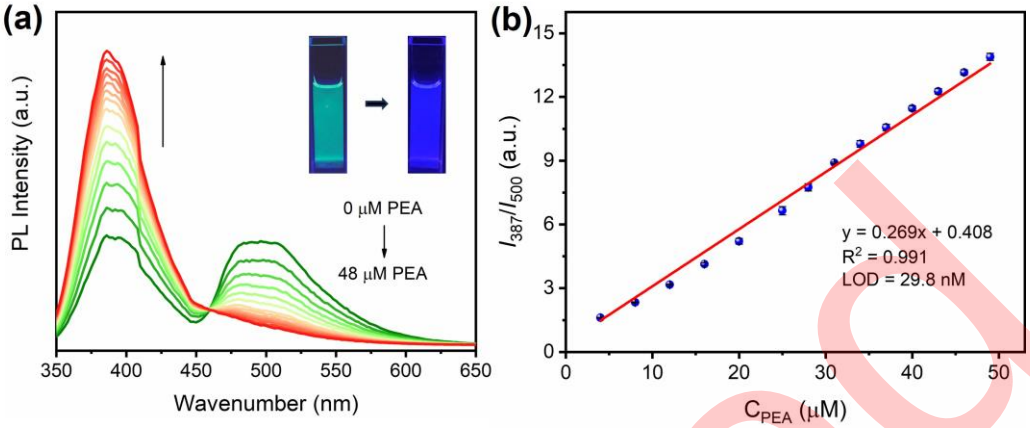

Figure S22. The ratiometric photoluminescence detection behavior of the $(BPBA)_2$·CB[8] toward PEA in urine. (a) The photoluminescence spectra (λ_{ex} = 345 nm) of $(BPBA)_2$·CB[8] suspension (16.7 μg/mL) upon the addition of PEA in urine. Inset: The photos of $(BPBA)_2$·CB[8] urine suspension before and after the addition of PEA. (b) Linear plot of I_{387}/I_{500} versus the concentrations of PEA (4-48 μM). Error bars represent mean ± s.d. (n = 3 independent experiments).

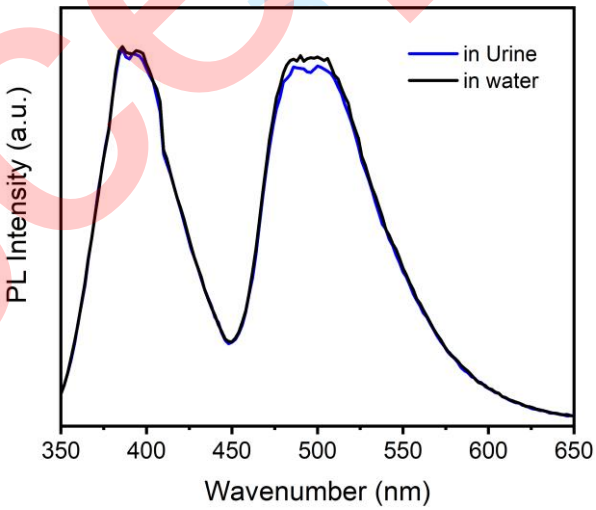

Figure S23. The photoluminescence spectra (λ_{ex} = 345 nm) of $(BPBA)_2$·CB[8] suspension (16.7 μg/mL) in water and in urine without PEA.

Table S4. Standard recovery for detecting PEA in urine (n=3).

Sample	Add (μM)	Found (μM)	Recovery (%)	RSD (%)
Urine	10	9.7	97.0	5.79

https://www.sciengine.com/doi/10.1007/s11426-024-2410-x
http://chem.scichina.com/english

20	19.5	97.5	7.12
40	40.8	102.0	8.20

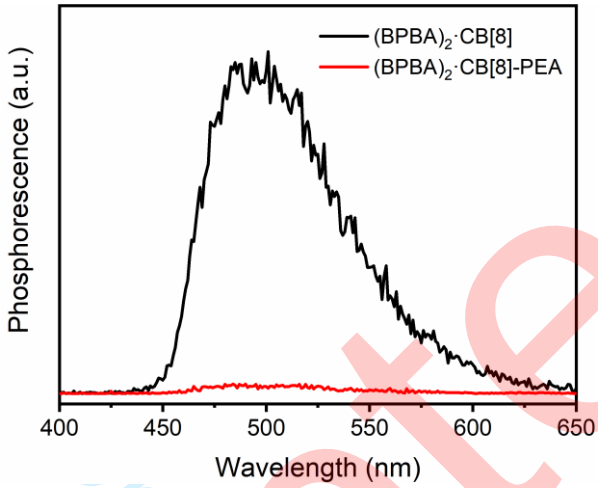

Figure S24. The RTP emission spectra of $(BPBA)_2$·CB[8] (16.7 μg/mL) before and after the addition of 48 μM PEA.

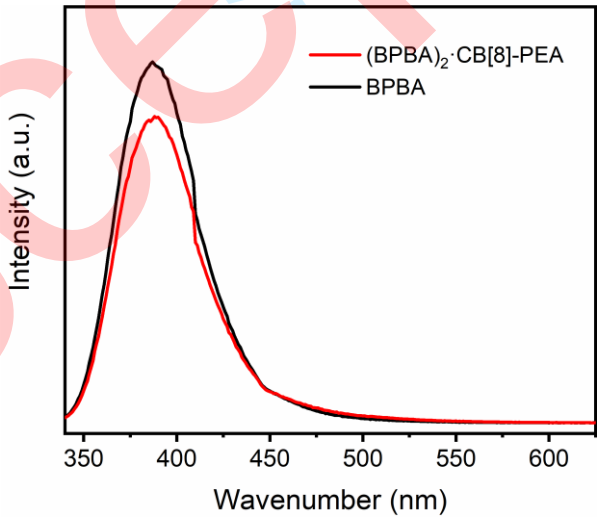

Figure S25. The photoluminescence spectra of free BPBA and $(BPBA)_2$·CB[8] (16.7 μg/mL) with the addition of 48 μM PEA.

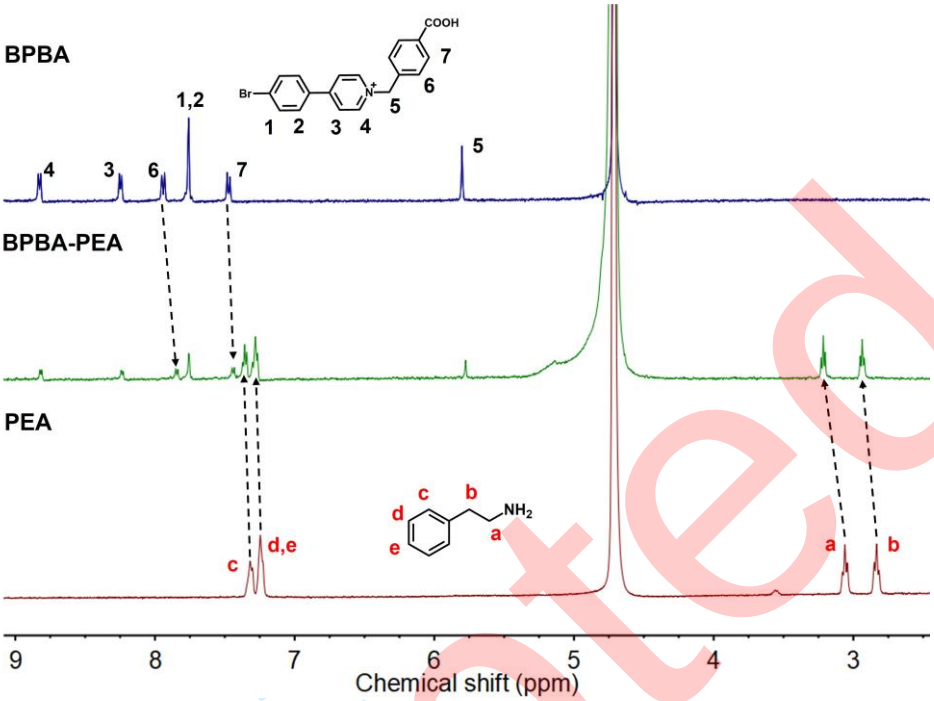

Figure S26. The ^{1}H NMR spectra of PEA, BPBA-PEA and BPBA ([PEA] = [BPBA] = 1.2 mM) (D_2O, 400 MHz, 298 K).

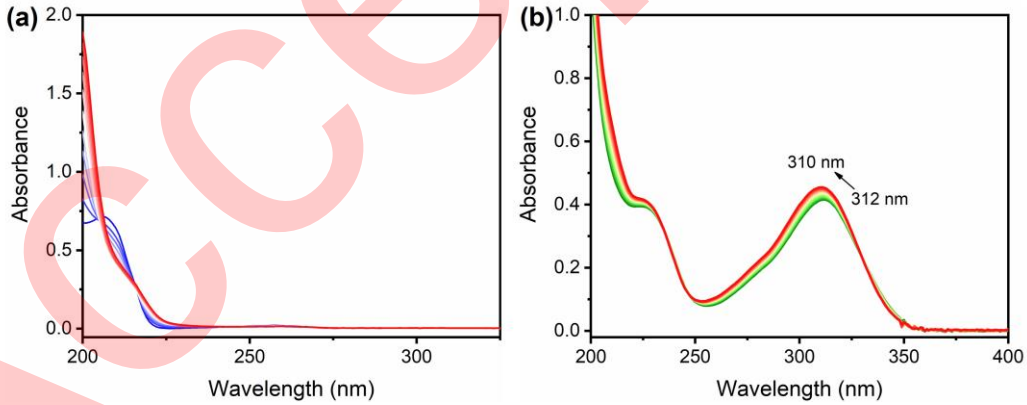

Figure S27. (a) The UV-vis absorption spectra of PEA with the addition of 0-1.0 eq. CB[8] ([PEA] = 0.1 mM). (b) The UV-vis absorption spectra of BPBA⊂CB[8] with the addition of 0-1.0 eq. PEA ([BPBA] = 2[CB[8]] = 20 μM).

References

1 Zhou W-L, Chen Y, Yu Q, Zhang H, Liu Z-X, Dai X-Y, Li J-J, Liu Y. *Nat. Commun.*, 2020, 11: 4655

2 Xu D-A, Zhou Q-Y, Dai X, Ma X-K, Zhang Y-M, Xu X, Liu Y. *Chin. Chem.*

Lett., 2022, 33: 851-854

3 Xu C, Yin C, Wu W, Ma X. *Sci. China Chem.*, 2022, 65: 75-81

4 Xing WW, Wang HJ, Liu Z, Yu ZH, Zhang HY, Liu Y. *Adv. Opt. Mater.*, 2023, 11: 2202588

5 Ma XK, Zhang W, Liu Z, Zhang H, Zhang B, Liu Y. *Adv. Mater.*, 2021, 33: 2007476

6 Yu H-J, Zhou Q, Dai X, Shen F-F, Zhang Y-M, Xu X, Liu Y. *J. Am. Chem. Soc.*, 2021, 143: 13887-13894

7 Su T, Liu Y-H, Chen Y, Liu Y. *J. Mater. Chem. C*, 2022, 10: 2623-2630

8 Ma X-K, Zhang Y-M, Yu Q, Zhang H, Zhang Z, Liu Y. *Chem. Commun.*, 2021, 57: 1214-1217

9 Zhou W-L, Lin W, Chen Y, Dai X-Y, Liu Z, Liu Y. *Chem. Sci.*, 2022, 13: 573-579

10 Liu Y-H, Tang M, Zhou X, Liu Y. *Mater. Adv.*, 2022, 3: 4693-4698

11 Liu Y-H, Liu Y. *J. Mater. Chem. B*, 2022, 10: 8058-8063

12 Zhou Y, Zhao D, Li Z-Y, Liu G, Feng S-H, Zhao B-T, Ji B-M. *Dyes Pigm.*, 2021, 195: 109725

13 Xu C, Lin X, Wu W, Ma X. *Chem. Commun.*, 2021, 57: 10178-10181

14 Zhang W, Luo Y, Liu C, Yang M-X, Gou J-X, Huang Y, Ni X-L, Tao Z, Xiao X. *ACS Appl. Mater. Interfaces*, 2022, 14: 51429-51437

15 Chen Y, Yang J, Zhang S, Xi Z, Luo H. *J. Inclu. Phenom. Macrocycl. Chem.*, 2022, 102: 429-437

16 Bhaumik SK, Panda SK, Banerjee S. *Chem. Commun.*, 2023, 59: 10396-10399

17 Dai X-Y, Song Q, Zhou W-L, Liu Y. *JACS Au*, 2023, 4: 216-227

18 Yin C, Yan ZA, Yan R, Xu C, Ding B, Ji Y, Ma X. *Adv. Funct. Mater.*, 2024, 2316008

https://www.sciengine.com/doi/10.1007/s11426-024-2410-x
http://chem.scichina.com/english

checkCIF/PLATON report

Structure factors have been supplied for datablock(s) BPBA-CB8

THIS REPORT IS FOR GUIDANCE ONLY. IF USED AS PART OF A REVIEW PROCEDURE FOR PUBLICATION, IT SHOULD NOT REPLACE THE EXPERTISE OF AN EXPERIENCED CRYSTALLOGRAPHIC REFEREE.

No syntax errors found. CIF dictionary Interpreting this report

Datablock: BPBA-CB8

```
Bond precision:   C-C = 0.0088 A          Wavelength=1.34139

Cell:           a=17.6926(16)     b=23.526(2)        c=27.594(2)
                alpha=96.294(3)   beta=103.719(3)    gamma=109.792(3)
Temperature:    150 K
```

	Calculated	Reported
Volume	10269.7(15)	10269.5(16)
Space group	P -1	P -1
Hall group	-P 1	-P 1
Moiety formula	4(C48 H48 N32 O16), 8(C19 H14 Br N O2), 61(H2 O) [+ solvent]	4(C19 H14 Br N O2), 4(C24 H24 N16 O8), 30.5(H2 O)
Sum formula	C344 H426 Br8 N136 O141 [+ solvent]	C172 H213 Br4 N68 O70.50
Mr	9361.41	4680.73
Dx,g cm-3	1.514	1.514
Z	1	2
Mu (mm-1)	1.216	1.216
F000	4850.0	4850.0
F000'	4854.86	
h,k,lmax	21,28,33	21,28,33
Nref	37642	37530
Tmin,Tmax	0.864,0.907	0.622,0.752
Tmin'	0.864	

```
Correction method= # Reported T Limits: Tmin=0.622 Tmax=0.752
AbsCorr = MULTI-SCAN

Data completeness= 0.997            Theta(max)= 53.907
```

```
R(reflections)= 0.0750( 23538)                          wR2(reflections)=
                                                        0.2367( 37530)
S = 1.068                    Npar= 2914
```

The following ALERTS were generated. Each ALERT has the format
test-name_ALERT_alert-type_alert-level.
Click on the hyperlinks for more details of the test.

Alert level B

```
PLAT420_ALERT_2_B D-H Bond Without Acceptor  O44      --H44B     .     Please Check
PLAT420_ALERT_2_B D-H Bond Without Acceptor  O45      --H45B     .     Please Check
PLAT420_ALERT_2_B D-H Bond Without Acceptor  O49      --H49C     .     Please Check
PLAT420_ALERT_2_B D-H Bond Without Acceptor  O54      --H54D     .     Please Check
PLAT430_ALERT_2_B Short Inter D...A Contact  O17      ..N54      .       2.87 Ang.
                                           -x,1-y,1-z   =      2_566 Check
```

Alert level C

```
PLAT241_ALERT_2_C High   'MainMol' Ueq as Compared to Neighbors of       C136 Check
PLAT241_ALERT_2_C High   'MainMol' Ueq as Compared to Neighbors of       C137 Check
PLAT241_ALERT_2_C High   'MainMol' Ueq as Compared to Neighbors of       C139 Check
PLAT241_ALERT_2_C High   'MainMol' Ueq as Compared to Neighbors of       C140 Check
PLAT241_ALERT_2_C High   'MainMol' Ueq as Compared to Neighbors of       C108 Check
PLAT241_ALERT_2_C High   'MainMol' Ueq as Compared to Neighbors of       C127 Check
PLAT242_ALERT_2_C Low    'MainMol' Ueq as Compared to Neighbors of       C135 Check
PLAT242_ALERT_2_C Low    'MainMol' Ueq as Compared to Neighbors of       C138 Check
PLAT242_ALERT_2_C Low    'MainMol' Ueq as Compared to Neighbors of       C153 Check
PLAT250_ALERT_2_C Large U3/U1 Ratio for <U(i,j)> Tensor(Resd    5)        2.2 Note
PLAT260_ALERT_2_C Large Average Ueq of Residue Including       O41      0.110 Check
PLAT260_ALERT_2_C Large Average Ueq of Residue Including       O42      0.101 Check
PLAT260_ALERT_2_C Large Average Ueq of Residue Including       O54      0.126 Check
PLAT260_ALERT_2_C Large Average Ueq of Residue Including       O55      0.131 Check
PLAT260_ALERT_2_C Large Average Ueq of Residue Including       O56      0.105 Check
PLAT260_ALERT_2_C Large Average Ueq of Residue Including       O73      0.103 Check
PLAT260_ALERT_2_C Large Average Ueq of Residue Including       O74      0.116 Check
PLAT334_ALERT_2_C Small <C-C> Benzene Dist.   C135     -C140     .       1.36 Ang.
PLAT341_ALERT_3_C Low Bond Precision on  C-C Bonds ...............    0.00885 Ang.
PLAT369_ALERT_2_C Long   C(sp2)-C(sp2) Bond  C169     - C172     .       1.56 Ang.
PLAT411_ALERT_2_C Short Inter H...H Contact  H12A     ..H24A     .       2.13 Ang.
                                           -x,2-y,2-z   =      2_577 Check
PLAT415_ALERT_2_C Short Inter D-H..H-X       H16A     ..H42C     .       2.01 Ang.
                                           1-x,2-y,2-z   =      2_677 Check
PLAT415_ALERT_2_C Short Inter D-H..H-X       H47C     ..H149     .       2.12 Ang.
                                                    x,y,z   =      1_555 Check
PLAT415_ALERT_2_C Short Inter D-H..H-X       H55C     ..H63      .       2.10 Ang.
                                                    x,y,z   =      1_555 Check
PLAT417_ALERT_2_C Short Inter D-H..H-D       H58A     ..H68A     .       2.14 Ang.
                                                    x,y,z   =      1_555 Check
PLAT906_ALERT_3_C Large K Value in the Analysis of Variance ......      3.416 Check
PLAT911_ALERT_3_C Missing FCF Refl Between Thmin & STh/L=    0.600        106 Report
               -2  2  0,  -1  2  0,   0  2  0,  -2  3  0,  -1  3  0,   6 18  0,
              -12 21  0, -11 21  0,   9-20  1,  10-20  1,   5 -5  1,   1 -3  1,
                2 -3  1,   0 -2  1,   1 -2  1,   2 -2  1,   1 -1  1,  -2  0  1,
                0  1  1,  -2  2  1,  -1  2  1,   0  2  1,  -2  3  1,  -1  3  1,
```

```
                -19 11  1, -12 21  1,  11-21  2,  10-20  2,   1 -3  2,   2 -3  2,
                 17 -3  2,   0 -2  2,   1 -2  2,   2 -2  2,   0 -1  2,   1 -1  2,
                  2 -1  2,   0  0  2,   1  0  2,   0  1  2,  -1  2  2,  -2  3  2,
                -17  5  2,  10 11  2,   4 17  2, -11 20  2,   1 -3  3,   0 -2  3,
                  1 -2  3,   0 -1  3,   1 -1  3,   2 -1  3,   3 -1  3,  -2  0  3,
                  0  0  3,   1  0  3,   2  0  3,   0  1  3,  -1  2  3,  -7  5  3,
                  9 11  3,   5 16  3,   2 18  3,  14 -4  4,  15 -4  4,   0 -2  4,
                  0 -1  4,  10  8  4,   9 10  4,   5 14  4,   6 14  4,   5 15  4,
                  4 16  4,   3 -4  5,  15 -4  5,   3 15  5,   0 19  5,  14 -4  6,
                  0 -3  6,   1  1  6,   6 10  6, -11 20  7,  11 -5  8,  -5 -3  8,
                  9-19  9, -12 20  9, -14 20 11,   8-18 12,   8 -5 15, -10 16 15,
                  9-18 17,   7-17 17,   8-17 17, -14 18 17, -12 21 17,   2-23 18,
PLAT971_ALERT_2_C Check Calcd Resid. Dens.  1.97Ang From O70              1.89 eA-3
PLAT971_ALERT_2_C Check Calcd Resid. Dens.  1.50Ang From O31              1.86 eA-3
PLAT971_ALERT_2_C Check Calcd Resid. Dens.  1.22Ang From O59              1.85 eA-3
PLAT971_ALERT_2_C Check Calcd Resid. Dens.  1.48Ang From O32              1.62 eA-3
PLAT971_ALERT_2_C Check Calcd Resid. Dens.  1.68Ang From O71              1.55 eA-3
PLAT975_ALERT_2_C Check Calcd Resid. Dens.  0.96Ang From O47      .       0.93 eA-3
PLAT975_ALERT_2_C Check Calcd Resid. Dens.  0.84Ang From O44      .       0.73 eA-3
PLAT975_ALERT_2_C Check Calcd Resid. Dens.  0.84Ang From O41      .       0.67 eA-3
PLAT975_ALERT_2_C Check Calcd Resid. Dens.  0.89Ang From O44      .       0.62 eA-3
PLAT976_ALERT_2_C Check Calcd Resid. Dens.  0.73Ang From O43      .      -0.74 eA-3
PLAT976_ALERT_2_C Check Calcd Resid. Dens.  0.45Ang From O43      .      -0.69 eA-3
PLAT976_ALERT_2_C Check Calcd Resid. Dens.  0.70Ang From O42      .      -0.68 eA-3
PLAT976_ALERT_2_C Check Calcd Resid. Dens.  0.79Ang From O42      .      -0.59 eA-3
PLAT976_ALERT_2_C Check Calcd Resid. Dens.  0.66Ang From O47      .      -0.56 eA-3
PLAT976_ALERT_2_C Check Calcd Resid. Dens.  1.00Ang From O27      .      -0.55 eA-3
PLAT976_ALERT_2_C Check Calcd Resid. Dens.  0.58Ang From O47      .      -0.54 eA-3
PLAT976_ALERT_2_C Check Calcd Resid. Dens.  0.75Ang From O50      .      -0.53 eA-3
PLAT977_ALERT_2_C Check Negative Difference Density on H05A       .      -0.37 eA-3
PLAT977_ALERT_2_C Check Negative Difference Density on H42D       .      -0.42 eA-3
PLAT977_ALERT_2_C Check Negative Difference Density on H43B       .      -0.32 eA-3
PLAT977_ALERT_2_C Check Negative Difference Density on H50B       .      -0.41 eA-3
PLAT977_ALERT_2_C Check Negative Difference Density on H51A       .      -0.39 eA-3
PLAT977_ALERT_2_C Check Negative Difference Density on H61D       .      -0.39 eA-3
```

Alert level G

```
ABSMU01_ALERT_1_G  Calculation of _exptl_absorpt_correction_mu
                   not performed for this radiation type.
PLAT002_ALERT_2_G Number of Distance or Angle Restraints on AtSite          2 Note
PLAT003_ALERT_2_G Number of Uiso or U(i,j) Restrained non-H Atoms           2 Report
PLAT007_ALERT_5_G Number of Unrefined Donor-H Atoms .............          70 Report
                H05A  H05B  H41C  H41D  H42C  H42D  H43A  H43B  H44A  H44B  H45A
                H45B  H46A  H46B  H47C  H47D  H48C  H48D  H49C  H49D  H50A  H50B
PLAT042_ALERT_1_G Calc. and Reported MoietyFormula Strings  Differ     Please Check
                Calc: 4(C48 H48 N32 O16), 8(C19 H14 Br N O2), 61(H2 O)
                Rep.: 4(C19 H14 Br N O2), 4(C24 H24 N16 O8), 30.5(H2
                      O)
PLAT045_ALERT_1_G Calculated and Reported Z Differ by a Factor ...      0.500 Check
PLAT072_ALERT_2_G SHELXL First  Parameter in WGHT  Unusually Large       0.13 Report
PLAT083_ALERT_2_G SHELXL Second Parameter in WGHT  Unusually Large       9.02 Why ?
PLAT154_ALERT_1_G The s.u.'s on the Cell Angles are Equal ..(Note)      0.003 Degree
PLAT172_ALERT_4_G The CIF-Embedded .res File Contains DFIX Records          1 Report
PLAT186_ALERT_4_G The CIF-Embedded .res File Contains ISOR Records          2 Report
PLAT187_ALERT_4_G The CIF-Embedded .res File Contains RIGU Records          1 Report
PLAT300_ALERT_4_G Atom Site Occupancy of O41        Constrained at        0.5 Check
```

```
PLAT300_ALERT_4_G Atom Site Occupancy of H41C       Constrained at        0.5 Check
PLAT300_ALERT_4_G Atom Site Occupancy of H41D       Constrained at        0.5 Check
PLAT300_ALERT_4_G Atom Site Occupancy of O44        Constrained at        0.5 Check
PLAT300_ALERT_4_G Atom Site Occupancy of H44A       Constrained at        0.5 Check
PLAT300_ALERT_4_G Atom Site Occupancy of H44B       Constrained at        0.5 Check
PLAT300_ALERT_4_G Atom Site Occupancy of O45        Constrained at        0.5 Check
PLAT300_ALERT_4_G Atom Site Occupancy of H45A       Constrained at        0.5 Check
PLAT300_ALERT_4_G Atom Site Occupancy of H45B       Constrained at        0.5 Check
PLAT300_ALERT_4_G Atom Site Occupancy of O56        Constrained at        0.5 Check
PLAT300_ALERT_4_G Atom Site Occupancy of H56A       Constrained at        0.5 Check
PLAT300_ALERT_4_G Atom Site Occupancy of H56B       Constrained at        0.5 Check
PLAT300_ALERT_4_G Atom Site Occupancy of O59        Constrained at        0.5 Check
PLAT300_ALERT_4_G Atom Site Occupancy of H59A       Constrained at        0.5 Check
PLAT300_ALERT_4_G Atom Site Occupancy of H59B       Constrained at        0.5 Check
PLAT300_ALERT_4_G Atom Site Occupancy of O70        Constrained at        0.5 Check
PLAT300_ALERT_4_G Atom Site Occupancy of H70A       Constrained at        0.5 Check
PLAT300_ALERT_4_G Atom Site Occupancy of H70B       Constrained at        0.5 Check
PLAT300_ALERT_4_G Atom Site Occupancy of O71        Constrained at        0.5 Check
PLAT300_ALERT_4_G Atom Site Occupancy of H71A       Constrained at        0.5 Check
PLAT300_ALERT_4_G Atom Site Occupancy of H71B       Constrained at        0.5 Check
PLAT300_ALERT_4_G Atom Site Occupancy of O72        Constrained at        0.5 Check
PLAT300_ALERT_4_G Atom Site Occupancy of H72C       Constrained at        0.5 Check
PLAT300_ALERT_4_G Atom Site Occupancy of H72D       Constrained at        0.5 Check
PLAT300_ALERT_4_G Atom Site Occupancy of O73        Constrained at        0.5 Check
PLAT300_ALERT_4_G Atom Site Occupancy of H73A       Constrained at        0.5 Check
PLAT300_ALERT_4_G Atom Site Occupancy of H73B       Constrained at        0.5 Check
PLAT302_ALERT_4_G Anion/Solvent/Minor-Residue Disorder (Resd   10)       100% Note
PLAT302_ALERT_4_G Anion/Solvent/Minor-Residue Disorder (Resd   13)       100% Note
PLAT302_ALERT_4_G Anion/Solvent/Minor-Residue Disorder (Resd   14)       100% Note
PLAT302_ALERT_4_G Anion/Solvent/Minor-Residue Disorder (Resd   25)       100% Note
PLAT302_ALERT_4_G Anion/Solvent/Minor-Residue Disorder (Resd   28)       100% Note
PLAT302_ALERT_4_G Anion/Solvent/Minor-Residue Disorder (Resd   39)       100% Note
PLAT302_ALERT_4_G Anion/Solvent/Minor-Residue Disorder (Resd   40)       100% Note
PLAT302_ALERT_4_G Anion/Solvent/Minor-Residue Disorder (Resd   41)       100% Note
PLAT302_ALERT_4_G Anion/Solvent/Minor-Residue Disorder (Resd   42)       100% Note
PLAT304_ALERT_4_G Non-Integer Number of Atoms in ..... (Resd   10)       1.50 Check
PLAT304_ALERT_4_G Non-Integer Number of Atoms in ..... (Resd   13)       1.50 Check
PLAT304_ALERT_4_G Non-Integer Number of Atoms in ..... (Resd   14)       1.50 Check
PLAT304_ALERT_4_G Non-Integer Number of Atoms in ..... (Resd   25)       1.50 Check
PLAT304_ALERT_4_G Non-Integer Number of Atoms in ..... (Resd   28)       1.50 Check
PLAT304_ALERT_4_G Non-Integer Number of Atoms in ..... (Resd   39)       1.50 Check
PLAT304_ALERT_4_G Non-Integer Number of Atoms in ..... (Resd   40)       1.50 Check
PLAT304_ALERT_4_G Non-Integer Number of Atoms in ..... (Resd   41)       1.50 Check
PLAT304_ALERT_4_G Non-Integer Number of Atoms in ..... (Resd   42)       1.50 Check
PLAT415_ALERT_2_G Short Inter D-H..H-X       H56A     ..H67A     .       2.00 Ang.
                                                1-x,2-y,1-z  =      2_676 Check
PLAT417_ALERT_2_G Short Inter D-H..H-D       H45A     ..H46A     .       2.00 Ang.
                                                         x,y,z  =      1_555 Check
PLAT417_ALERT_2_G Short Inter D-H..H-D       H45A     ..H46B     .       1.97 Ang.
                                                         x,y,z  =      1_555 Check
PLAT417_ALERT_2_G Short Inter D-H..H-D       H69B     ..H70A     .       2.01 Ang.
                                                         x,y,z  =      1_555 Check
PLAT432_ALERT_2_G Short Inter X...Y Contact  Br2      ..C65      .       3.33 Ang.
                                               -x,2-y,1-z  =      2_576 Check
PLAT432_ALERT_2_G Short Inter X...Y Contact  Br3      ..C88      .       3.27 Ang.
                                                         x,y,z  =      1_555 Check
PLAT432_ALERT_2_G Short Inter X...Y Contact  Br4      ..C2       .       3.29 Ang.
```

```
                                                  x,y,-1+z  =      1_554 Check
PLAT432_ALERT_2_G Short Inter X...Y Contact  O1       ..C160     .       2.91 Ang.
                                                -x,2-y,1-z  =      2_576 Check
PLAT432_ALERT_2_G Short Inter X...Y Contact  O05S     ..C31      .       2.90 Ang.
                                                  x,y,-1+z  =      1_554 Check
PLAT432_ALERT_2_G Short Inter X...Y Contact  O2       ..C164     .       2.88 Ang.
                                                -x,2-y,1-z  =      2_576 Check
PLAT432_ALERT_2_G Short Inter X...Y Contact  O3       ..C39      .       2.97 Ang.
                                                    x,y,z   =      1_555 Check
PLAT432_ALERT_2_G Short Inter X...Y Contact  O3       ..C38      .       3.01 Ang.
                                                    x,y,z   =      1_555 Check
PLAT432_ALERT_2_G Short Inter X...Y Contact  O11      ..C107     .       2.86 Ang.
                                                    x,y,z   =      1_555 Check
PLAT432_ALERT_2_G Short Inter X...Y Contact  O13      ..C103     .       2.82 Ang.
                                                    x,y,z   =      1_555 Check
PLAT432_ALERT_2_G Short Inter X...Y Contact  O17      ..C88      .       2.90 Ang.
                                                -x,1-y,1-z  =      2_566 Check
PLAT432_ALERT_2_G Short Inter X...Y Contact  O17      ..C84      .       2.93 Ang.
                                                -x,1-y,1-z  =      2_566 Check
PLAT432_ALERT_2_G Short Inter X...Y Contact  O23      ..C141     .       2.93 Ang.
                                                -x,1-y,1-z  =      2_566 Check
PLAT432_ALERT_2_G Short Inter X...Y Contact  O35      ..C125     .       3.00 Ang.
                                                -x,1-y,1-z  =      2_566 Check
PLAT432_ALERT_2_G Short Inter X...Y Contact  O38      ..C57      .       3.01 Ang.
                                                    x,y,z   =      1_555 Check
PLAT432_ALERT_2_G Short Inter X...Y Contact  O39      ..C122     .       3.00 Ang.
                                                -x,1-y,1-z  =      2_566 Check
PLAT432_ALERT_2_G Short Inter X...Y Contact  O45      ..C68      .       3.01 Ang.
                                                    x,y,z   =      1_555 Check
PLAT432_ALERT_2_G Short Inter X...Y Contact  O48      ..C46      .       2.97 Ang.
                                                    x,y,z   =      1_555 Check
PLAT432_ALERT_2_G Short Inter X...Y Contact  O61      ..C50      .       2.89 Ang.
                                                    x,y,z   =      1_555 Check
PLAT605_ALERT_4_G Largest Solvent Accessible VOID in the Structure        138 A**3
PLAT720_ALERT_4_G Number of Unusual/Non-Standard Labels .........          3 Note
              O05S    H05A    H05B
PLAT790_ALERT_4_G Centre of Gravity not Within Unit Cell: Resd.  #          5 Note
              C19 H14 Br N O2
PLAT790_ALERT_4_G Centre of Gravity not Within Unit Cell: Resd.  #         13 Note
              H2 O
PLAT790_ALERT_4_G Centre of Gravity not Within Unit Cell: Resd.  #         15 Note
              H2 O
PLAT790_ALERT_4_G Centre of Gravity not Within Unit Cell: Resd.  #         16 Note
              H2 O
PLAT790_ALERT_4_G Centre of Gravity not Within Unit Cell: Resd.  #         17 Note
              H2 O
PLAT790_ALERT_4_G Centre of Gravity not Within Unit Cell: Resd.  #         18 Note
              H2 O
PLAT790_ALERT_4_G Centre of Gravity not Within Unit Cell: Resd.  #         19 Note
              H2 O
PLAT790_ALERT_4_G Centre of Gravity not Within Unit Cell: Resd.  #         20 Note
              H2 O
PLAT790_ALERT_4_G Centre of Gravity not Within Unit Cell: Resd.  #         21 Note
              H2 O
PLAT790_ALERT_4_G Centre of Gravity not Within Unit Cell: Resd.  #         22 Note
              H2 O
PLAT790_ALERT_4_G Centre of Gravity not Within Unit Cell: Resd.  #         29 Note
```

```
              H2 O
PLAT790_ALERT_4_G Centre of Gravity not Within Unit Cell: Resd.  #          30 Note
              H2 O
PLAT790_ALERT_4_G Centre of Gravity not Within Unit Cell: Resd.  #          35 Note
              H2 O
PLAT790_ALERT_4_G Centre of Gravity not Within Unit Cell: Resd.  #          40 Note
              H2 O
PLAT790_ALERT_4_G Centre of Gravity not Within Unit Cell: Resd.  #          41 Note
              H2 O
PLAT790_ALERT_4_G Centre of Gravity not Within Unit Cell: Resd.  #          42 Note
              H2 O
PLAT860_ALERT_3_G Number of Least-Squares Restraints ............        2551 Note
PLAT868_ALERT_4_G ALERTS Due to the Use of _smtbx_masks Suppressed          ! Info
PLAT910_ALERT_3_G Missing # of FCF Reflection(s) Below Theta(Min).          4 Note
               -1  1  0,   0  1  0,   0 -1  1,   0  0  1,
PLAT913_ALERT_3_G Missing # of Very Strong Reflections in FCF ....          1 Note
                5 -5  1,
PLAT933_ALERT_2_G Number of HKL-OMIT Records in Embedded .res File          5 Note
               -5 -3  8,   0 -3  6,  -7  5  3,   3 -4  5,  -2  0  1,
PLAT941_ALERT_3_G Average HKL Measurement Multiplicity ..........        3.5 Low
PLAT969_ALERT_5_G The 'Henn et al.' R-Factor-gap value ..........      3.552 Note
              Predicted wR2: Based on SigI**2  6.66 or SHELX Weight 22.17
PLAT978_ALERT_2_G Number C-C Bonds with Positive Residual Density.          0 Info

------------------------------------------------------------------------------
   0 ALERT level A = Most likely a serious problem - resolve or explain
   5 ALERT level B = A potentially serious problem, consider carefully
  50 ALERT level C = Check. Ensure it is not caused by an omission or oversight
 106 ALERT level G = General information/check it is not something unexpected

   4 ALERT type 1 CIF construction/syntax error, inconsistent or missing data
  81 ALERT type 2 Indicator that the structure model may be wrong or deficient
   7 ALERT type 3 Indicator that the structure quality may be low
  67 ALERT type 4 Improvement, methodology, query or suggestion
   2 ALERT type 5 Informative message, check
------------------------------------------------------------------------------
------------------------------------------------------------------------------
```

It is advisable to attempt to resolve as many as possible of the alerts in all categories. Often the minor alerts point to easily fixed oversights, errors and omissions in your CIF or refinement strategy, so attention to these fine details can be worthwhile. In order to resolve some of the more serious problems it may be necessary to carry out additional measurements or structure refinements. However, the purpose of your study may justify the reported deviations and the more serious of these should normally be commented upon in the discussion or experimental section of a paper or in the "special_details" fields of the CIF. checkCIF was carefully designed to identify outliers and unusual parameters, but every test has its limitations and alerts that are not important in a particular case may appear. Conversely, the absence of alerts does not guarantee there are no aspects of the results needing attention. It is up to the individual to critically assess their own results and, if necessary, seek expert advice.

Publication of your CIF in IUCr journals

A basic structural check has been run on your CIF. These basic checks will be run on all CIFs submitted for publication in IUCr journals (*Acta Crystallographica*, *Journal of Applied Crystallography*, *Journal of Synchrotron Radiation*); however, if you intend to submit to *Acta Crystallographica Section C* or *E* or *IUCrData*, you should make sure that full publication checks are run on the final version of your CIF prior to submission.

Publication of your CIF in other journals

Please refer to the *Notes for Authors* of the relevant journal for any special instructions relating to CIF submission.

PLATON version of 13/05/2024; check.def file version of 04/05/2024

Datablock BPBA-CB8 - ellipsoid plot